DESIGN AND DEVELOPMENT OF A MICROCAVITY HOLLOW CATHODE GLOW DISCHARGE EMISSION SYSTEM FOR SIMULTANEOUS MULTIELEMENT ANALYSIS OF DISCRETE NANOSAMPLES OF SOLUTION RESIDUES

BY

CHERYL MORGAN

A DISSERTATION PRESENTED TO THE GRADUATE SCHOOL OF THE UNIVERSITY OF FLORIDA IN PARTIAL FULFILLMENT OF THE REQUIREMENTS FOR THE DEGREE OF DOCTOR OF PHILOSOPHY

UNIVERSITY OF FLORIDA

1993

To Will, Dale and Barney - thanks for keeping my spirits up

ACKNOWLEDGMENTS

It is with a great sense of accomplishment and pride that I finish up my studies at the University of Florida. A graduate degree in chemistry seemed almost an impossible dream 5 or 6 years ago. But with a great deal of encouragement from my undergradnate chemistry professors, Dr. David Burgess and Dr. William Totherow, I took the plnnge and entered gradnate school in the fall of 1989. It has not always been easy for me bnt with friends like Rachel Gagnon, how could I have given up? My family has shown me a great deal of support. My parents, Ellie and Bing Lonnroth, helped me get off to a good start in Florida. My children Laurie and Brian have stoyed by my side and have given me three beautiful grandchildren - Alexis, Andrew and Jamie. My wonderful grandmother, Evelyn Leard, has been a saint (I love you!). My husband, Will Morgan, has been an anchor for me. His nndying love and support are with me daily. My brother, Dale Lonnroth, has been my number one cheerleader. His faith in me throughout the years has sustained my spirit and focused my energies. My thanks to a great friend.

In addition to my family and friends, I gratefully acknowledge the support and encouragement from my advisors and coworkers. My sincere thanks go to my

research advisor, Dr. Jim Winefordner, for his guidance and support of my research. I would also like to thank Ben Smith. His experimental expertise was invaluable. Cheryl Davis was a great help and support with this project. Bill Spencer graciously allowed me to share the photodiode array system with him. It was a pleasure to work alongside Mike Wensing in CLB 207. Finally, thanks go to Ben Womack who took me under his wing when I first joined the group. It has been a great research group to work with.

TABLE OF CONTENTS

Abstract of Dissertation Presented to the Graduate School
of the University of Florida in Partial Fulfillment of the
Requirements for the Degree of Doctor of Philosophy

DESIGN AND DEVELOPMENT OF A MICROCAVITY HOLLOW CATHODE GLOW DISCHARGE EMISSION SYSTEM FOR SIMULTANEOUS MULTIELEMENT ANALYSIS OF DISCRETE NANOSAMPLES OF SOLUTION RESIDUES

By

Cheryl Morgan

August, 1993

Chairman Prof James D Winefordner
Major Department Chemistry

The hollow cathode glow discharge is a rather modest atomic emission source, but, nevertheless has many desirable characteristics The discharge is easy to initiate and maintain, providing sharp atomic lines with a low background continuum The low pressure environment virtually eliminates chemical reactions, matrix effects and self absorption. The nonthermal sputtering atomization process yields an atom cloud representative of the bulk material

Although theoretically the hollow cathode glow discharge is nearly an ideal source, in reality it has suffered from weak signal output It has been shown that cathode geometry plays an important role in the atomic emission signal intensity

The hollow cathode geometry increases the emission sensitivity over the planar cathode, but not enough to rival other atomic emission sources. The work presented in this dissertation focuses on the use of a microcavity hollow cathode glow discharge (MCHCGD) as a method to enhance signal output.

Although there are several effective multielement techniques in use today, they all require large sample volumes. There are circumstances, however, in which only a very small sample may be available (i.e. forensic samples and precious bodily fluids) but the determination of many elements on the trace and ultratrace level may be required. This project investigates the applicability of MCHCGD to the simultaneous multielement analysis of discrete nanosamples of solution residues.

Several important diagnostic parameters were determined, including pressure, voltage, current, sample drying time, slit width and chamber purging.

The experimental investigation was performed in two phases. The first phase evaluated the MCHCGD emission system as a source for ultratrace analysis. Single element analysis of Cu and Pb was performed using each element's strongest emission line. The limits of detection, 2 pg for Cu and 36 fg for Pb, demonstrated that the MCHCGD is an excellent source for ultratrace analysis. The second phase evaluated the MCHCGD emission system as a multielement source. Simultaneous determination of Pb, V, and Cr was achieved, demonstrating that the MCHCGD is a good multielement source.

CHAPTER 1
INTRODUCTION

Overview of the Glow Discharge

The glow discharge is a rather modest quasi-plasma which is generated upon spark breakdown between two electrodes immersed in a low pressure, rare gas environment. It is a self-sustaining discharge easily maintainable under a certain set of conditions -pressures ranging from 1-10 Torr, applied voltages ranging from 400-2000 V and currents ranging from 1-1000 mA, depending on the rare gas-cathode material combination.

In this low pressure environment, the glow discharge is virtually free from self-absorption and self reversal.[1] It yields narrow spectral lines[2] and provides an atom cloud representative of the bulk material being sampled[3] with atom densities ranging from 10^{9} - 10^{16} cm^{-3}.[4]

The ground state free atom population, necessary for atomic emission studies, is generated by a nonthermal, nonselective sputtering process. Because the sputtering process is non-thermal, many of the interferences associated with thermally excited sources, such as matrix effects and sample vaporization, are not associated with the d.c. glow discharge. The subsequent excitation of the free particles sputtered from the solid matrix occurs as a result of the energy generated

in an electric field Consequently the glow discharge falls into the category of electric discharges The categories of atomic emission sources are presented in Table 1-1

Table 1-1 Categories of Atomic Emission Sources

- Thermal Sources
  - High Temperature Furnaces
  - Flames
- Electric Discharge Sources
  - Low Pressure
    - Arcs
    - Glow Discharges
      - Planar Cathode
      - Hollow Cathode
      - Geissler Electrodeless
  - Atmospheric Pressure
    - Arcs
      - d c Arcs
      - High Voltage a c Arcs
    - Sparks
    - Plasmas
      - Blown Arcs
        - Atomic Hydrogen
        - Plasmatrons
      - RF Discharges
        - Inductive
        - Capacitive
      - Microwave Discharges
        - Capacitive
        - Microwave Induced

Although the glow discharge is a [illegible] plasma, both in [illegible] energy,[5] it has been shown to be an effective radiation source and has been successfully coupled to a wide variety of detection systems for use in atomic absorption,[6-10] atomic fluorescence [11-14] atomic emission,[15-17] resonance ionization[18] and mass spectrometry [19-23] Applications for the glow discharge source have been extensive and include analysis of metal alloys,[24-25] determination of gases in metals [26] determination of trace metals in biological tissues,[27] analysis of solution residues[28-29] and impurity analysis of thin films and semiconductors [30-31]

One of the reasons for the wide applicability of the glow discharge is the broad range of excitation energies achievable with the use of different noble gases Table 1-2 lists the energies of the long-lived triplet metastable levels characteristic of all the noble gases These triplet states are associated with the excitation of the analyte atoms [31] Any element with an excitation potential at or below the excitation potential of the noble gas is able to be collisionally excited by the noble gas Nearly all of the elements are excitable by one or more of the noble gases

Table 1 2 Excitation Potentials of the Noble Gases[32]

Noble Gas	Excitation Threshold (eV)
Helium	20 55, 19 77
Argon	11 49, 11 86
Neon	16 62, 16 72
Krypton	9 86, 10 51
Xenon	8 28, 9 40

History

The glow discharge is not a new analytical tool. On the contrary, it has been widely investigated since 1916 when Friedrich Paschen first explored its potential as a spectral source. Paschen fashioned a Geissler tube with an open-ended aluminum hollow cylinder to serve as the cathode. Upon evacuation of the tube below 1 Torr, and with a sufficient applied voltage, he observed a glow wholly contained within the hollow cylinder. He varied the pressure and current density until a stable discharge was achieved and recorded the emission spectrum of helium. Paschen is credited with the first application of the glow discharge source to spectroscopic analysis.[33-34]

Since Paschen's groundbreaking work, the glow discharge has enjoyed a steady, albeit sporadic, evolution. In 1928, Takahashi[35] reported on fundamental studies of the excitation processes in the hollow cathode glow discharge source. Sawyer[36] added to the knowledge of glow discharges with his studies on cathode materials and carrier gases. Schüler's research[37] in the late 1920's focused on the detailed spectral analysis of hyperfine structures as well as the usefulness of the hollow cathode glow discharge for analyzing small samples.[38] After a 13-year period of inactivity in glow discharge research, McNally[39] published the results of quantitative studies on cathode materials. This was the first work that proved a direct relationship between signal intensity and the amount of sputtered material. McNally's results sparked a renewed interest in the glow discharge and led to a

period of intense investigation of the glow discharge throughout the 1950s and 1960s

In the 1950s, the research primarily focused on using the hollow cathode glow discharge tube as a source for atomic absorption studies [40] In the 1960s, the Russians investigated the hollow cathode glow discharge as an atomic emission source[41] while Winefordner[42] paved the way for glow discharge atomic fluorescence In 1968 Grimm[43] introduced a glow discharge source which combined the best characteristics of planar and hollow cathode designs The Grimm glow discharge source extended the applicability of glow discharge spectrometry to a wide variety of solid conducting samples as well as non conducting powders [44] A typical Grimm type glow discharge is illustrated in Figure 1-1 (from Human[4])

The 1970s was a decade of waning interest in glow discharge research The source had proved highly suitable for atomic absorption spectroscopy but was disappointingly inadequate as an atomic emission source More robust and powerful atomic emission sources, like the inductively coupled plasma, were capturing the interest of research groups around the world Problems with designing demountable hollow cathodes for rapid sample analysis were the major stumbling blocks to further development of the glow discharge source There were also problems with contamination of the carrier gas by air and water vapor as well as difficulty maintaining stringent vacuum requirements.

Figure 1-1 Schematic cross section of a Grimm-type glow discharge

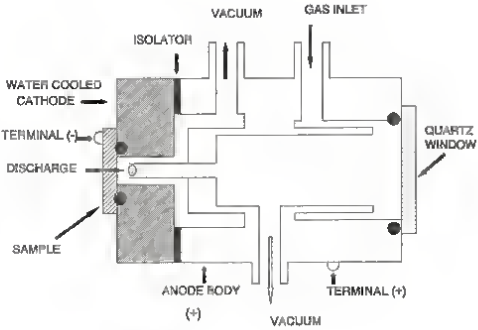
VACUUM
GAS INLET
ISOLATOR
WATER COOLED
CATHODE
TERMINAL (-)
DISCHARGE
QUARTZ
WINDOW
SAMPLE
ANODE BODY
(+)
TERMINAL (+)
VACUUM

Interest was again sparked in the 1980s as researchers turned their attention back to investigating the hollow cathode discharge as a spectral source. Up until this time, the advantages of the glow discharge, i.e. high excitation efficiency, high stability, low background intensity, narrow spectral linewidths, low cost and absence of matrix interferences and thermal effects, led investigators to believe the glow discharge might prove to be an ideal source. In actual performance, it was disappointing because the major disadvantage found in working with the hollow cathode glow discharge was its comparatively weak signal output. Research over the past decade has focused on improving the source to overcome this disadvantage with the expectation that it could be used for trace and ultratrace analysis.

Recent Developments in Hollow Cathode Glow Discharge Instrumentation

As previously stated, recent modifications of the hollow cathode glow discharge instrumentation have been aimed at enhancing the analytical signal output.

One signal boosting technique that has been very successful has been to couple the glow discharge to another form of external energy. Caroli[45,46] has successfully coupled the hollow cathode glow discharge with a 2450 MHz microwave generator. There are basically two electron populations in the glow discharge - fast electrons responsible for collisional ionization and the less energetic slow electrons responsible for excitation processes. Coupling the two excitation sources, the microwave plasma and the glow discharge, results in a

higher density of fast electrons, which, in turn, increases ionization of rare gas as well as the density of metastable species. The increase in metastable rare gas atoms eventually leads to an increase in analyte excitation through Penning ionization processes. The analytical signal is enhanced by at least an order of magnitude while the intensity of the background spectrum of the noble gas is lessened. Kruger[47] and Sacks[48-49] both applied an external magnetic field to the hollow cathode glow discharge. It was found that the magnetic field did not affect the motion of the atoms and ions, the electron density, the excitation cross section of the levels, the mean free path of the electrons, the spontaneous radiation, the background continuum or the quenching collisions. It did, however, affect the motion of the charged particles in the plasma, causing the high energy beam electrons to migrate to the chamber walls, allowing the low energy electrons, responsible for the excitation processes, to predominate. It was demonstrated that with an increase in the external magnetic field, the analytical signal, as well as the discharge current, showed an increase while the noble gas line intensities remained unchanged. Decreases in limits of detection using this technique range from 1-2 orders of magnitude.

Another boosting technique that has attracted a great deal of interest is the RF-boosted pulsed hollow cathode glow discharge. In this technique, a current pulse is applied to the discharge followed by a short burst of rf energy. The atom cloud produced by the current pulse is subsequently re-excited by the rf burst

Araki[50] and Farnsworth[51] had good success with this technique, reporting a 5 times signal enhancement when sampling the rf burst versus the current pulse.

Since cathode geometry has been shown to have a significant effect upon signal output,[43] boosting techniques which alter the cathode geometry have also been investigated, the most important of which is the use of a microcavity hollow cathode. The microcavity hollow cathode refers to hollows of less than 2 mm in diameter. Novolsielov and Znamienskii[52] developed an empirical formula to express the relationship between the spectral line intensity (I_o) and the cathode diameter (d)

$$I_o d = k \qquad (1)$$

where k is a constant. Experimental data has confirmed that the smaller the diameter of the hollow, the greater the spectral line intensity. This holds true for hollows less than 2 mm in diameter with a length-to-diameter ratio of at least 3:1. Several phenomena are responsible for the two order of magnitude decrease in detection limits using this cathode.[45] The small cavity size decreases the electron energy allowing the low energy excitation processes to dominate. There is also an increase in the concentration of the sputtered species, an increase in the current density and an increase in the residence times of the analyte. Any one of these phenomena would certainly increase the intensity of the emission signal, together they have a dramatic affect. The microcavity hollow cathode glow discharge is the focus of the work detailed in this dissertation.

Scope of Dissertation

There are several effective analytical techniques in use today which allow for simultaneous multielement analysis, including inductively coupled plasma atomic emission spectroscopy, inductively coupled plasma mass spectrometry, microwave plasma techniques and flame emission. As effective as these methods may be, they all require large sample volumes. There are circumstances, however, in which a multielement analysis on the trace or ultratrace level is required but only a small sample is available for the analysis, i.e. forensic samples and precious bodily fluids. The need for a technique which can analyze discrete microliter/nanoliter samples for many elements simultaneously is evident. The development of this microcavity hollow cathode glow discharge emission system is in response to this need.

The first chapter of this dissertation will introduce the glow discharge as an analytical source and present an overview of the historical background of the hollow cathode glow discharge. Recent developments in signal enhancement techniques will also be discussed. An in-depth discussion of the fundamental processes that occur in the glow discharge will be presented in chapter 2. In chapter 3, the details of the design and development of a microcavity hollow cathode glow discharge emission system will be highlighted. Chapter 4 will focus on two series of experiments involving single element determination of copper and lead in nanoliter sized solution residues using the microcavity. The results

presented in this chapter will support the contention that the microcavity hollow cathode glow discharge is an excellent source for ultratrace analysis. Chapter 5 will highlight a series of experiments designed to analyze nanoliter sized samples for more than one element at a time. The results presented in this chapter will support the contention that the microcavity hollow cathode glow discharge is an excellent multielement source. Chapter 6 will pull together the results from chapters 3-5 and will make the case that the microcavity hollow cathode glow discharge emission system shows great promise as a valid multielement technique for discrete nanoliter samples. Future work and improvements to the system will also be discussed.

CHAPTER 2
LOW PRESSURE DISCHARGES

Discharge Features and Characteristics

Types of Low Pressure Discharges

There are several types of gaseous discharges that can be generated between two electrodes in a low pressure rare gas environment. Figure 2-1 plots the voltage-current characteristics of four of them.

The first type of discharge, the Townsend discharge, is described by region AB in figure 2-1, and is a dark, non self-sustaining discharge. The voltage that is applied to the cathode creates an electric field between the electrodes. Electrons emitted by the cathode migrate toward the anode. In traversing the distance between the cathode and anode, a number of electron impact ionization collisions occur with the rare gas atoms. The positive ions thus created are swept toward the negatively charged cathode. In a Townsend discharge, there is a steady-state relationship between newly created ions and the discharge current. The number of ions arriving at the cathode is exactly equal to the number of electrons impinging on the anode. Since this type of discharge is entirely dependent upon an external ionization source (the applied voltage to the cathode) and, in fact, extinguishes immediately upon its removal, the Townsend discharge is not a self-

Figure 2 1 Voltage current characteristics of low pressure discharges [54]

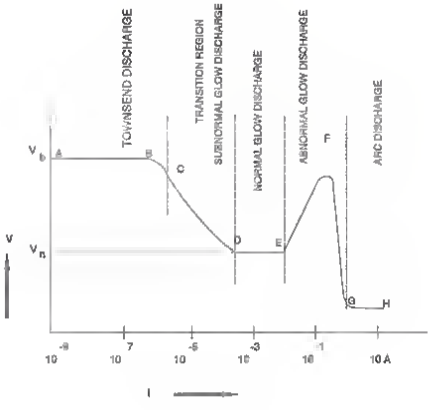
TOWNSEND DISCHARGE
TRANSITION REGION
SUBNORMAL GLOW DISCHARGE
NORMAL GLOW DISCHARGE
ABNORMAL GLOW DISCHARGE
ARC DISCHARGE
V
I
A
B
C
D
E
F
G
H

sustaining discharge. This type of discharge can only be generated at very low currents where the positive ion space-charge distortion of the field is relatively small.[5]

In the second section of figure 2-1, CD, it is clear that with an increase in current at the same pressure comes a change in the voltage. As the current within the discharge increases, there is an increase in ionization within the discharge. The voltage required to sustain the discharge subsequently decreases as the number of electrons which carry the current increases. At this point, there is an onset of what is called an electron avalanche and electron multiplication begins to take place. The voltage-current characteristics of region CD do not describe a type of discharge but rather a transition region between the dark non self-sustaining discharge to a luminous self sustaining discharge.

The next type of low pressure discharge depicted in figure 2-1 begins at point D, where, with an increase in current, the normal cathode fall potential, V_{nf} is reached and a visible glow is observed. This type of discharge is called a "normal glow discharge." The current is now sufficient for stable electron multiplication to occur. Under these conditions, a self-sustaining luminous discharge, not solely dependent upon an external ionization source, is generated. This means that each electron emitted by the cathode causes secondary processes to occur in the active region of the discharge, which result in the original electron being replaced by a newly emitted electron from the cathode. In this "normal

glow discharge" regime the cathode fall potential is maintained at 200 300 V and remains constant even with large increases in current, from 10^{-4} to 0 1 A.

Upon additional increases in current, the current density physically expands across the cathode surface until the surface is saturated At this point, E in figure 2-1, any increase in current results in an increase in voltage This kind of discharge is referred to as an "abnormal glow discharge" and is the type of low pressure discharge most often used in glow discharge work

The last type of low pressure discharge represented in figure 2-1 is the arc discharge As can be seen in region FGH, an increase in current results in a sudden drop in voltage to only tens of volts The arc discharge is characterized by high current and low voltage. Electron emission from the cathode is primarily the result of thermionic emission, as opposed to the other low pressure discharges, where electron emission occurs as a result of a cathodic sputtering

Features of the Abnormal Glow Discharge

The abnormal glow discharge hereinafter referred to simply as the glow discharge, is generated by passing an electric current through a rare gas under low pressure The elementary processes which occur in the gaseous medium as a result of this electrical disturbance are numerous and complex Penning[54] enumerated the various processes which are summarized in Figure 2 2

Visually, the glow discharge has a distinct structure of alternating zones of varying luminosity[55] These zones are best understood by analyzing the structure

Figure 2-2 Schematic diagram of elementary processes in a glow discharge.[54]

CATHODE (-)
ELECTRONS
RECOMBINATION
IONIZATION
EXCITATION
FAST ATOMS
POS. IONS
RADIATION
EXCITATION
ELASTIC COLLISION
HEAT
IONIZATION
NEG. IONS
ELECTRONS
ANODE (+)

of a glow discharge generated between two plane parallel electrodes as depicted in Figure 2-3. Each zone represents an area of the discharge undergoing characteristic physical processes, i.e. excitation and ionization.[56]

Close to the cathode is a thin layer called the Aston dark space. Low energy electrons emitted by the cathode via secondary emission begin their journey to the anode in this space. Carman[57-59] has recently modeled the Aston dark space and has concluded that the electrons are emitted from the cathode with a range of energies from 0 to 14 eV. Although the electrons maintain this range of energies throughout most of the Aston dark space, they begin to pick up energy and momentum as they are repelled from the negatively charged cathode.

In the adjacent cathode glow region, the electrons have gained enough energy to cause some collisional excitation of the rare gas atoms. A very weak glow is observed in this region. The cathode glow is also a very small region of the glow discharge. Its thickness is dependent upon the type of rare gas and the gas pressure.[53]

Since the glow discharge is a self-sustaining discharge and the electrons necessary to sustain the glow come from interactions between the cathode material and the rare gas rather than from thermionic emission, there must be a region in the discharge where ionization of the rare gas atoms and electron multiplication take place. This region is known, variously, as the cathode dark space, Crooke's dark space or Hittorf dark space. The cathode dark space follows the cathode

Figure 2 3 Representation of the main features of a planar glow discharge

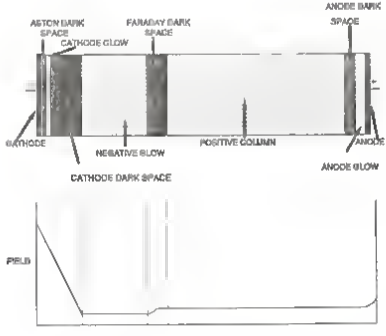
ANODE DARK SPACE
ASTON DARK SPACE
FARADAY DARK SPACE
CATHODE GLOW
CATHODE
NEGATIVE GLOW
POSITIVE COLUMN
ANODE
ANODE GLOW
CATHODE DARK SPACE
PIELS

glow region and represents the point where the electrons are so energetic they cause collisional ionization rather than collisional excitation. The cathode dark space carries almost the entire cathode fall potential of the discharge[60] through an initially high and then linearly descending electric field.[61] This causes the positive ions to stream toward the negatively charged cathode and the electrons to be ejected into the next region of the discharge, the negative glow. This is an ongoing process and since the electron mobility is so much greater than the ion mobility, the cathode dark space is a region of high positive ion density.[62] Toward the anode side of the cathode dark space, the electron density increases.[63] Overall, the cathode dark space is the most important zone of the glow discharge and is essential for maintaining the current flow.[64]

In a planar cathode glow discharge, there are two distinct populations of electrons which emerge from the cathode dark space and enter the negative glow. Those electrons which have accelerated across the cathode drop without undergoing inelastic collisions enter the negative glow with energies upwards of 150-200 eV. These fast beam electrons are responsible for the ionization processes at the very beginning of the negative glow region. They penetrate only a short distance, 1-2 mm,[65] before they lose their energy, mainly through inelastic collisions with rare gas atoms. The second population of electrons are the slow plasma electrons with energies ranging from 0.1 to 50 eV. These electrons come from two sources. A small number of electrons emitted from the cathode, which

have undergone inelastic collisions before reaching the negative glow, enter this region with energies ranging from 0.1 to 1 eV [66]. The great majority of plasma electrons come from ionization processes within the first mm of this region as the beam electrons are injected into the negative glow. The range of energies of these plasma electrons is from 10 to 50 eV [67]. The plasma electrons are responsible for the excitation processes that occur in the negative glow. Since they are, by far, the most abundant type of electrons in this zone, the negative glow is the most luminous region of the entire discharge. The great majority of the slow plasma electrons have sufficient energy to cause excitation of the rare gas atoms and ions as well as resonance transitions of most of the elements. Clearly, this is the region of interest for spectral analysis.

The negative glow is actually a neutral plasma with rather high, 10^{11} to 10^{14} cm^{-3}, but approximately equal concentrations of positive ions and electrons. The ground state argon atom population here has been shown to be on the order of 10^{13} to 10^{16} cm^{-3} making the net ionization degree somewhat less than 1% [67]. The ground state analyte atom population has been measured at values from 10^{9} to 10^{16} cm^{-3} [5,6,13,17,45].

The electric field in the negative glow is very low and nearly uniform throughout. This very low field gradient is also indicative of a neutral conductive[53] plasma region.

Physical studies of the negative glow have yielded good information about the diffusion processes that govern this plasma region. One important measurement in determining the diffusion processes present in a discharge is the Debye length. This varies as the square root of the ratio of the electron temperature to the electron density [68]. In the negative glow, the electron temperature as well as the electric field is low[65,69] compared to a rather high electron density, 10^{11} to 10^{14} cm^{-3}, thus making the Debye length very small. When the Debye length is small compared to the dimensions of the glow discharge chamber, radial diffusion losses of charged particles are governed by ambipolar diffusion [70]. This theory holds true for the negative glow region.

Immediately following the negative glow is the Faraday dark space (FDS). This region is characterized by a slight rise in field as the electron population diminishes and additional voltage is needed to sustain the current flow. The FDS is comprised of ground state particles and low energy electrons which have lost their energy in the collisionally active negative glow region. This region is a transition region between two plasma zones, the negative glow and the positive column. The boundaries of the FDS are not clearly defined but blend into the adjacent plasmas.

Studies of the FDS show it to be a region of decreasing electron density from the high densities in the negative glow to the low densities in the positive column. The field as well as the electron temperature increase toward the positive

column The Debye length is on the order of 10^{-3} cm making this a quasineutral region not governed by ambipolar diffusion theory [71] The flow of electrons is dictated by drift flow in the field gradient

Having gained enough energy (20 eV)[67] in the increasing FDS field, the electrons are accelerated toward the anode producing the luminous positive column along the way As previously stated, the positive column is the second plasma region in the glow discharge It is much less luminous than the negative glow, but can be much larger in size depending upon the separation between the cathode and the anode The length of the cathode region (Aston dark space, cathode glow, cathode dark space and negative glow) is dependent upon the type and the pressure of the rare gas at a given voltage On the other hand, the length of the positive column and the FDS are determined by the separation between the electrodes If a glow discharge is generated in a long tube, such as a neon light the positive column is the glow that is observed throughout most of its length. However, since neither the FDS nor the positive column are actually necessary to produce or maintain the glow discharge, they can be totally eliminated by placing the anode at the end of the negative glow region This produces an obstructed glow discharge and is the basis for the successful Grimm type glow discharge The minimum separation between the electrodes for the formation of a stable discharge is about twice the thickness of the cathode dark space [72]

The positive column is characterized by a low voltage gradient and a reduced electron density, 10^8 cm^{-3}.[59] A spectral examination of the radiation from the positive column shows emission emanating from low energy atomic transitions with almost no emission from ions. Most of the energy loss in this region occurs at the walls of the chamber due to ambipolar diffusion of ions.[75] Comparatively little energy is lost to radiation.

The anode region of the glow discharge consists of an anode dark space and an anode glow region. As electrons emerge from the positive column and stream toward the anode, they are initially low enough in energy that they are unable to excite the neutral gas atoms in the area. There is almost no glow in this region, thus the name anode dark space. The electrons do, however, pick up enough energy for excitation as they accelerate toward the anode and a glow region can be observed immediately adjacent to the anode.

Characteristics of the Abnormal Glow Discharge

With the fundamental work of Paschen, Sawyer, Schüler, McNally and others, the glow discharge was long ago proven to be a good spectroscopic source. Since that time, it has been extensively studied and very well characterized, as illustrated in Figure 2-4.

As can be seen in figure 2-4 (a), radiation from the glow discharge is most intense in the two plasma regions, the negative glow and the positive column. Every zone in the discharge is, however, luminous to some extent. The dark

zones only appear nonluminous in contrast to the brightly glowing regions. The negative glow is the region of spectral interest with emission lines emanating from both atomic and ionic transitions.

The distribution of the electric field in the glow discharge is very interesting. Figure 2-4 (b) shows the major fields, which are confined to areas close to the electrodes, as well as a minimal field throughout the plasma regions of the discharge. There are two observed field reversals.[68] The first one occurs close to the negative glow region where the field decreases as the electron density gradient increases. In this region, no electric field is needed to carry the axial current. Ambipolar diffusion sweeps the electrons along axially and the positive ions radially. The second field reversal occurs in the Faraday dark space where there is a diminution of the electron population due to radial diffusion losses. Here an increase in the field is necessary to maintain the current flow.

The positive, negative and net space charges, illustrated in figure 2-4 (c), (d), and (e), correspond to the physical processes occurring in the various regions as described in the previous section.

The current density is illustrated in figure 2-4 (f) showing regions of ionic (i^+) current and electronic (i^-) current.

Another aspect of interest is the distribution of gas temperature throughout the discharge, as shown in figure 2-4 (g). A plot of the temperature vs. distance from the cathode shows the areas where energy is lost to heating of the gas. The

Figure 2-4 Characteristics of a planar glow discharge [53-54]

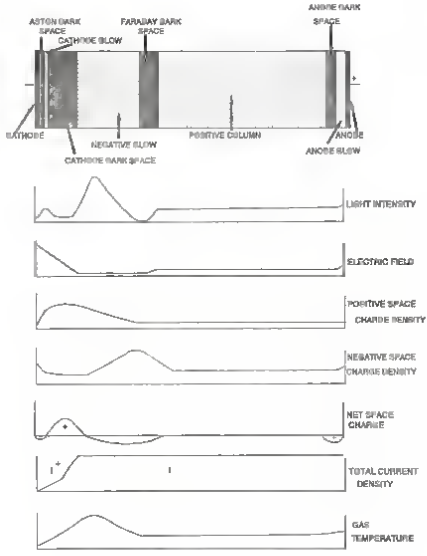
ASTON DARK SPACE
CATHODE GLOW
FARADAY DARK SPACE
ANODE DARK SPACE
+
CATHODE
NEGATIVE GLOW
CATHODE DARK SPACE
POSITIVE COLUMN
ANODE
ANODE GLOW
LIGHT INTENSITY
ELECTRIC FIELD
POSITIVE SPACE CHARGE DENSITY
NEGATIVE SPACE CHARGE DENSITY
NET SPACE CHARGE
+
TOTAL CURRENT DENSITY
I
I+
GAS TEMPERATURE

gas temperature in the negative glow is approximately 1000 K[53] and in the positive column approximately 300 K.

Cathodic Sputtering

One of the most important advantages of using the glow discharge as a spectral source is its nonthermal sputtering atomization process.

In a low pressure environment, the negatively charged cathode is subjected to severe positive ion bombardment. A transfer of momentum takes place[74] between the incident ion and a matrix particle (i.e. neutral atom, ion, cluster or electron) through a collisional cascade.[75-78] If a sufficient amount of energy is transferred to the target atom to overcome the matrix-particle binding energy, a surface particle will be ejected. Figure 2.5 illustrates this sputtering process. Over 90% of the sputtered particles are ground state neutral atoms. A few percent are ions and a small fraction may be clustered particles.[15]

Because sputtering is essentially a nonthermal process, thermal evaporation of the sample contributes <0.1% to the primary release of surface particles.[77]

Sputtering efficiency, or sputtering yield, is a measure of the number of sputtered particles per incident ion. It is dependent upon the energy of the impacting ion as well as the rare gas-analyte combination. The energy of the impacting ion is determined by the external applied voltage. The higher the voltage, the higher the cathode fall potential and the more energetic the ion. The total discharge potential is not solely comprised of the cathode fall potential

Figure 2.5 Schematic representation of the sputtering process

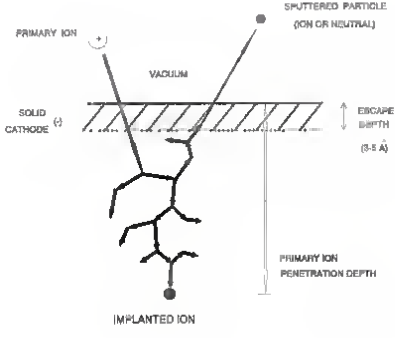
SPUTTERED PARTICLE
(ION OR NEUTRAL)
PRIMARY ION
VACUUM
SOLID
CATHODE
ESCAPE
DEPTH
(3-5 Å)
PRIMARY ION
PENETRATION DEPTH
IMPLANTED ION

There is a small plasma potential associated with the secondary processes in the discharge It is, however, insignificant (1-4 V) compared to the external applied voltage (400-2000 V) and can be neglected [78] The ion energy can be considered equal to the applied voltage

Studies have shown that the impacting ion must have a minimum threshold energy of between 15 and 35 eV in order to effect release of a target atom [64 77] The sputtering yield then increases linearly up to impacting energies on the order of 100 eV The yield then levels off and decreases at very high impact energies (1 keV)[79] at which point, the incident ion penetrates too deeply into the matrix and no sputtering takes place [77] The sputtering yield is also affected by the masses of the analyte atom and the incident ion The yield has been found to increase with increasing mass of the impacting ion achieving a maximum yield when the masses of the impacting ion and the target atom are the same [41]

The sputtering yield in atoms per incident ion, S, can be determined by considering the energy E, and mass dependence of the incident ion, m , and target atom m_i, system [75]

$$S = \frac{3\sigma}{4\pi} \frac{4m m_i}{(m_i+m)^2} \frac{E}{U_o} \qquad (2)$$

In this expression, U_o represents the surface binding energy (eV), E is the energy of the incident ion (eV), σ is a monotonic increasing function of the ratio m_i/m and equal to 0 17 if the ratio is 0 1 and increasing to 1 4 for m_i/m = 10

Equation 1 predicts a linear relationship between the sputtering yield and the energy of the incident ion and holds true for pure metals and incident ion energies up to 1 keV. It also predicts an inverse relationship between the sputtering yield and the surface binding energy or sublimation energy.

Cathode Geometry

Hollow Cathode

The discussion of the features and characteristics of the glow discharge thus far presented applies to glow discharges generated between planar cathodes. Studies have shown that by altering the geometry of the cathode from a planar configuration to a hollow cylinder, the emission intensity increases by 2-3 orders of magnitude [30-32]. This "hollow cathode effect" is wholly a result of the altered geometry of the cathode. The same regions and characteristics of the planar cathode glow discharge occur in the hollow cathode glow discharge but they are arranged differently. The regions necessary for the production and maintenance of the discharge, namely the cathode sheath and negative glow, are contained within the hollow, while the anode regions (the FDS, the positive column, the anode dark space and the anode glow) are external to the cavity.

To illustrate how this type of discharge develops, a study was performed which replaced the single planar cathode with a U-shaped cathode, the opening of which faced the anode [1]. The discharge features were monitored as a function of the separation of the side arms of the U-shaped cathode. In effect, it was like

placing two flat cathode discharges parallel to each other, reducing the separation between them and then observing the resultant discharge. At an arm separation of 25 mm, the discharge appeared to be two distinct discharges separated by a dark space in the center. The emission intensity was comparable to a discharge with a single planar cathode. When the separation between the arms of the U-shaped cathode was decreased to 8 mm or less, the two negative glow regions were observed to coalesce into a single much brighter discharge. Overlapping the negative glow regions had a dramatic effect on the emission intensity. Measurements of emission line intensities showed a 200- to 1000-fold increase in the signal.

The geometrical configuration most widely used to achieve this hollow cathode effect is the hollow cylinder, with one or both ends open. The cathode layers which are observed in the planar glow discharge are also present in the cavity of the hollow cathode, but are arranged in a circular manner as shown in Figure 2-6.

Electrons emitted from the cathode traverse a narrow, 0.05-0.07 mm,[83-84] cathode sheath region (Aston dark space, cathode glow, and cathode dark space). Because of some of the physical processes that occur in the hollow cathode glow discharge, this cathode sheath region is much smaller than the similar region of a planar glow discharge. The electrical characteristics, however, are the same. The electric field is initially very high and decreases linearly with distance from the

Figure 2.6 Representation of a hollow cathode glow discharge

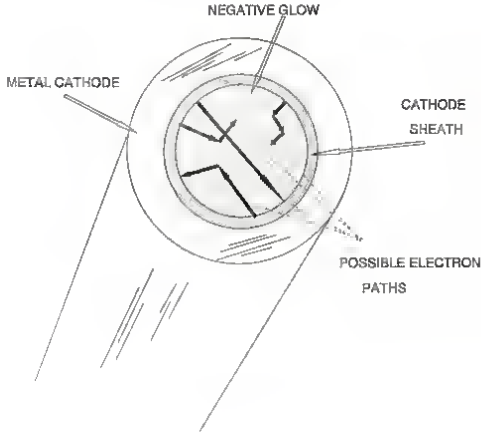
NEGATIVE GLOW
METAL CATHODE
CATHODE
SHEATH
POSSIBLE ELECTRON
PATHS

cathode surface to near zero at the negative glow region The cathode dark space carries almost the entire cathode fall potential as it does with a planar cathode However, since it has to carry this potential through a much smaller distance, the field gradient is much steeper, which results in ions having a higher average energy as they strike the surface of the cathode resulting in increased sputtering yields

Studies on the energies of electrons entering the negative glow region in a hollow cathode glow discharge indicate the presence of three distinct populations,[72,85-86] as opposed to the planar cathode glow discharge, where most authors refer only to the fast and slow electrons In the hollow cathode glow discharge, the very fast beam electrons enter the negative glow after having been accelerated across the entire cathode drop without having undergone any (or many) inelastic collisions Therefore, they have energies comparable to the full cathode fall potential (> 150 eV) They are responsible for the ionization processes in the negative glow The fast or secondary electrons arrive in the negative glow with much less energy than the beam electrons This population of electrons derives from ionization processes at the beginning of the negative glow and has a range of energies from 3 15 eV Finally, there are the plasma electrons These are the electrons which have become thermalized to the temperature of the plasma through multiple inelastic collisions These electrons are the most abundant group of electrons in the negative glow and are responsible for much of the excitation

The geometry of the cathode has an effect on the behavior of the electrons. It has been found that the mean free path of the electrons in a hollow cathode glow discharge is on the order of the diameter of the cathode cavity.[5,67,87] Because of this, many of the high energy beam electrons cross the negative glow collision free and enter the cathode sheath on the opposite side of the hollow cathode. Once inside the cathode sheath, these electrons reverse direction and are reinjected into the negative glow resulting in multiple passes through this region. It has been shown that the beam electrons oscillate between the walls of the cathode, undergoing repeated cycles of excitation while confined in the cavity. After a time, they thermalize and eventually diffuse to the anode.[88]

The geometry of the hollow cathode also affects the species reaching the cathode surface. In planar glow discharges, one of the processes by which an electron is emitted from the cathode surface is photoemission. Photons emitted from the glowing regions of the discharge are not affected by electric fields and therefore have a small random probability of reaching the cathode surface, depending on the area of the planar cathode. With the hollow cathode configuration, there is only a small chance that a photon will travel anywhere but to the cathode surface. With a hollow cathode glow discharge, the negative glow clearly has more contact area with the surface of the cathode. Also, the hollow cathode discharge is much brighter than the planar glow discharge, consequently, more photons are produced. It has been shown that photoemission can be a major

contributor to secondary electron ejection from the cathode [5,89] The likelihood of a photon striking the surface of the cathode increases from 0.3 in a planar cathode glow discharge to 0.8 in a hollow cathode glow discharge.[90] Not only are photons more likely to strike the surface of the cathode but back diffusion of analyte particles ionized in the cathode dark space is also greatly enhanced using the hollow cathode configuration This is due mainly to the increase in electron impact collisions and is highly dependent upon gas pressure The cathode geometry traps all the species present in the cathode sheath and negative glow regions within the hollow electrons ions atoms, metastables, photons[91-92] increasing the residence time in the analytical zone The escape rate for rare gas and analyte species is less than 2% that of a planar cathode glow discharge system [93] Just as in the planar cathode glow discharge, the negative glow region of the hollow cathode glow discharge is governed by ambipolar diffusion The difference is that the ions which diffuse radially in the planar cathode glow discharge are lost to analysis on the walls of the chamber, whereas the ions which diffuse radially in the hollow cathode glow discharge diffuse to the cathode sheath and are subsequently accelerated to the cathode walls by the strong electric field, making them available for re-sputtering [93]

The current density within the hollow cathode glow discharge has been shown to be non uniform and concentrated toward the bottom of the hollow [94-95] Such a current density gradient increases the sputtering rate [96]

Overall, it has been found that the increase in the emission signal using the hollow cathode configuration can be attributed to an increase in ionization in the negative glow, an increase in photoemission of secondary electrons from the cathode surface, an increase in residence times of analyte species, and an increase in sputtering rates and analyte vapor concentration

Microcavity Hollow Cathode

In Chapter 1, section 1 3, an overview of signal enhancement techniques for the hollow cathode glow discharge was presented One of the most promising techniques mentioned was the use of a microcavity hollow cathode This technique was said to offer a two order of magnitude improvement in detection limits over conventional hollow cathode glow discharges The work presented in this dissertation makes use of the microcavity hollow cathode With some understanding of hollow cathode glow discharges, it now seems appropriate to examine the microcavity hollow cathode in more detail

Clearly the same basic properties and characteristics of the hollow cathode glow discharge apply to the microcavity hollow cathode glow discharge Studies have shown that with the reduced diameter, the effects are even more pronounced [97-100] First of all, the smaller cavity increases the analyte concentration in the negative glow region There is also an increase in pressure within the hollow It has been shown that the product of the pressure,p, and the diameter of the cavity, d_c, is a constant,[5, 97] so that as the diameter decreases the pressure

increases The smaller cavity size means that there will be a thinner cathode sheath, resulting in a greater effect of the electric field in the cathode dark space From this, increased sputtering rates can be expected along with a more concentrated atom cloud

All of these observations are valid but do not account for the dramatic increase in emission intensity when the diameter of the cathode is reduced, for example, from 3 mm to 2 mm This same dramatic increase in emission intensity is not observed when the diameter of the hollow is reduced from 5 mm to 4 mm or from 4 mm to 3 mm The "microcavity effect" is only observed in hollows less than 2 mm in diameter with a length-to-diameter ratio of at least 3 1 Unfortunately, there has been no theoretical treatment of the microcavity effect in the literature and, so, this phenomenon remains unexplained

Excitation and Ionization Processes in the Hollow Cathode Glow Discharge

The negative glow region of the hollow cathode glow discharge is the most important region for spectral analysis Ground state analyte atoms sputtered from the surface of the cathode are available for excitation or ionization by a number of different processes

The principal mechanism responsible for excitation occurs by way of electron impact processes with electrons of low or moderate energy [101] The mechanisms which result in ionization are more complicated In some parts of the discharge, electron impact by high energy electrons causes ionization In other

parts, ionization can be due to charge transfer reactions or to Penning ionization by metastable rare gas atoms [102-105]. Table 2-2[67] summarizes some of the important excitation and ionization processes that occur in the negative glow region.

Table 2-2 Glow Discharge Excitation and Ionization Mechanisms

	EXCITATION
Electron Impact	$A\ (or\ X) + e \rightarrow A^*\ (or\ X^*) + e$ $A^+\ (or\ X^+) + e \rightarrow A^{*+}\ (or\ X^{*+}) + e$
Photoexcitation	$A\ (or\ X) + h\nu \rightarrow A^*\ (or\ X^*)$
	IONIZATION
Penning	$X^m + e \rightarrow X^+ + 2e$ $X^m + A^* \rightarrow X + A^+ + e$ $X^m + A \rightarrow X + A^{*+} + e$ $X^m + A^* \rightarrow X^* + A^+ + e$
Charge Transfer	$X^+ + A \rightarrow X + A^+$

X = rare gas atom
X^m = rare gas metastable atom
X^+ = rare gas ion
X^* = excited rare gas atom

A = analyte atom
A^+ = analyte ion
A^* = excited analyte atom
A^{*+} = excited analyte ion

CHAPTER 3
DESIGN AND PARAMETRIC EVALUATION OF A MICROCAVITY HOLLOW CATHODE GLOW DISCHARGE EMISSION SYSTEM

Chamber and Cathode Design

In approaching the task of designing a glow discharge chamber incorporating a microcavity hollow cathode, the goals of the design strategy had to be developed and evaluated in light of previous and current research in the field. The first goal was to reduce the physical size of the chamber itself. Previous work performed in our laboratory[106] using a 6 way stainless steel vacuum cross (260 cm^3 volume) as the glow discharge chamber concluded that the large chamber volume contributed greatly to analyte vapor dilution. It was observed that, upon ignition of the discharge, the atom cloud immediately diffused away from the planar cathode to the walls of the chamber, decreasing the concentration of the analyte species in the probe volume of this glow discharge laser excited atomic fluorescence system. Becerra[106] recommended construction of a mini glow discharge chamber to increase the concentration of the analyte vapor cloud and to reduce diffusion of the analyte away from the cathode. Although this recommendation applied to a planar cathode glow discharge, it seemed appropriate to investigate a reduced chamber size for the proposed microcavity hollow cathode.

glow discharge atomic emission system. The smaller chamber size, it was theorized, might favorably alter the diffusion dynamics both internally and externally for the microcavity hollow cathode glow discharge. It was decided that the new chamber would be approximately one third the volume of the chamber used in Becerra's work. Since Becerra made atomic emission measurements using a hollow cathode as well as atomic fluorescence measurements using a planar cathode with the large chamber, a direct comparison could be made to determine if the reduced size of the chamber influenced the analytical figures of merit.

The second goal of the chamber design plan was to build an inexpensive, simple to operate, emission source, so that modifications, should they become necessary, could be made easily and inexpensively. It was determined that the chamber and cathodes could be made by modifying 19/22 and 19/38 pyrex tapered joints. The outer joint could be fashioned into the chamber and the inner joint could be made into a cathode. These tapered joints fit snugly together, allowing the vacuum criteria to be met.

The next thing to consider was the placement of the gas inlet, the vacuum outlet and the anode. The vacuum outlet was placed at the end of the chamber next to the viewing port. Since this would increase the gas flow close to the window, it was hoped that this arrangement would help to prevent or reduce sample deposition on the viewing window. The anode was placed opposite the vacuum port and was recessed to avoid physically obstructing the emission signal.

The placement of the gas inlet took a little more thought. Traditionally, the gas inlet has been placed close to and parallel with the viewing window. This allowed the stream of carrier gas to flow across the window surface in an effort to prevent or reduce sample deposition on the viewing window. Many chambers incorporate this design.[23,61,66,107,110] In 1976, however, Gough[11] developed a jet-assisted glow discharge in which he changed the position of the gas inlet. His glow discharge chamber design positioned the gas inlet very close to and parallel with the surface of a planar cathode to prevent impurities from depositing on the cathode surface. Since that time, the jet-assisted glow discharge has been utilized by a few investigators with good success.[12, 15] They found that this configuration increased sputtering rates and transport of species away from the cathode. They also found that back diffusion onto the cathode surface was reduced. It was decided to incorporate this design feature in the new microcavity glow discharge emission system. Since the sample sizes which were to be analyzed would be less than 200 ng, for the largest of the samples, it was predicted that sample deposition on the chamber viewing window would only be a minor problem. It was felt that it was more important to make every effort to increase sputtering rates so that the sample would be completely removed in as short a period of time as possible.

Figure 3-1 is an illustration of the new chamber design.

The last goal of the new design involved the microcavity hollow cathode. The cathode had to be easily demountable and interchangeable to expedite the

Figure 3-1. Schematic diagram of glow discharge chamber

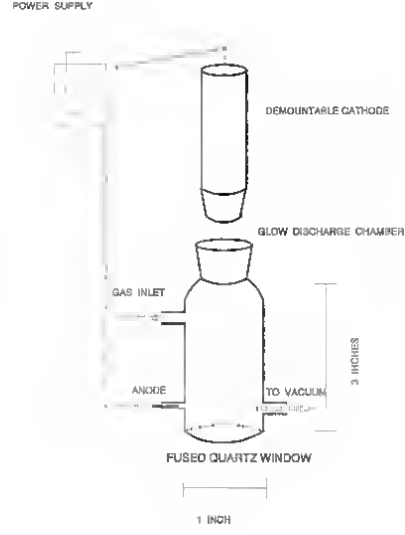
POWER SUPPLY
DEMOUNTABLE CATHODE
GLOW DISCHARGE CHAMBER
GAS INLET
ANODE
TO VACUUM
3 INCHES
FUSED QUARTZ WINDOW
1 INCH

sample analysis procedure. Figure 3-2 illustrates the design of the cathode that was finally decided upon. Each metal microcavity hollow cathode would first be machined to specifications (1.5 - 2.0 mm dia. x 6 mm deep). The metal microcavity cathode would be epoxied into a ceramic sleeve fashioned from machineable Macor. The ceramic sleeve would electrically isolate the metal cathode and confine the discharge within the cavity. The ceramic-sheathed metal cathode would then be epoxied into a 19/38 pyrex inner tapered joint and would be affixed with an appropriate electrical connection to the negative pole of the high voltage power supply. It was felt that these cathodes would prove to be easy to make and easy to ignite.

The performance of this first chamber and cathode design was very good, but there was a problem with overheating of the cathode. After just a few minutes of continuous use, the cathodes would heat up too much, causing the ceramic to expand and cracking the pyrex inner tapered joint. Eventually, the chamber cracked and broke as well. A new chamber was fashioned from a quartz 19/22 outer tapered joint and new cathodes were built using quartz 19/38 inner tapered joints. The basic design of the chamber and cathode remained the same.

Experimental Setup

A schematic diagram of the experimental setup is presented in Figure 3-3. As can be seen from this illustration, the experimental setup is a simple one. The entire arrangement, in fact, fits on one 4' x 6' optical bench.

Figure 3-2 Schematic diagram of the microcavity hollow cathode


19/39 QUARTZ INNER TAPERED JOINT
CERAMIC SLEEVE
METAL CATHODE
ELECTRICAL CONNECTION

Figure 3-3 A schematic diagram of the experimental setup

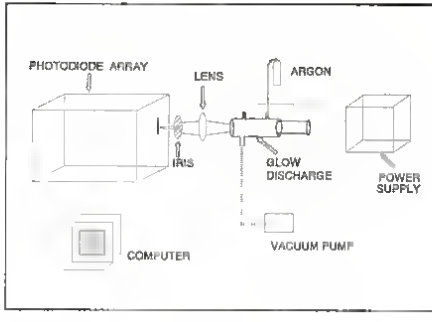
PHOTODIODE ARRAY
LENS
ARGON
IRIS
GLOW
DISCHARGE
POWER
SUPPLY
COMPUTER
VACUUM PUMP

The microcavity hollow cathode glow discharge source, which is the heart of this project, was mounted with a sturdy laboratory constructed Teflon ring holder on an x-y-z stage to simplify the alignment procedure. The cathode was connected to the negative terminal of a high voltage power supply (Hippotronics, Inc., Model 803-330, Brewster, NY) which ranged in voltage up to 3000 V and current up to 400 mA. The anode, machined from stainless steel, was epoxied into a 7/15 quartz outer tapered joint built into the glow discharge chamber and was electrically grounded. In order to limit the current going through the discharge and improve discharge stability, a 3.115 kΩ ballast resistor was connected in series with the power supply. A laboratory constructed toggle switch, which enabled remote ignition of the glow discharge, was also connected to the power supply.

A dual stage rotary pump (Leybold Heraus Vacuum Products, Inc., Model Trivac A, Export, PA) was used to evacuate the glow discharge chamber. A capacitance manometer was used for monitoring the chamber pressure. Argon, the carrier gas used in these studies, was supplied to the glow discharge chamber via a gas inlet located near the cathode. The argon flow into the chamber was regulated at 2 mL/min with a precision needle valve. A pressure gauge was mounted between the needle valve and the argon tank so that the pressure to the needle valve could be controlled separately from the argon tank pressure.

To provide some external cooling to the cathode, a length of 1/8 inch i d Tygon tubing was connected to a flowing chilled water supply and wound around the outside of the chamber neck where the cathode is inserted

Complicated optics were unnecessary with this system The emission output of the microcavity glow discharge was focused onto the entrance slit of the monochromator through a 3" focal length planoconvex lens An aperture, reduced to the size of the focused beam, was placed directly in front of the spectrometer slit to prevent stray light from reaching the detector Occasionally, neutral density filters were used, and when this was necessary, they were mounted in front of the aperture

The wavelength dispersion system used in the project was a 1-meter spectrometer (Jobin-Yvon model HR1000, Princeton, NJ – 2400 grooves mm^{-1}, linear dispersion of 0 5 nm mm^{-1}) The detection system was an intensified photodiode array (Princeton Instruments Inc– OSMA Model IR4 1024, Princeton, NJ) Data acquisition and processing was controlled with the use of a personal computer and OSMA I-120 software With this instrument, the signal can either be integrated over a selected period of time or a selected number of scans can be accumulated If desired both integration and accumulation can be performed on the same signal

Parametric Evaluation of a Microcavity Hollow Cathode Glow Discharge System

As with any new analytical system, the microcavity hollow cathode glow discharge emission system used in this work needed to be optimized. The various parameters essential for ensuring peak performance of the system were defined and a series of optimization experiments were performed. The project plan called for investigation of the microcavity hollow cathode glow discharge as a source for simultaneous multielement analysis of discrete nanoliter samples of solution residues. There were to be two phases of the study. The first phase was designed to determine if the microcavity hollow cathode glow discharge was an effective source for ultratrace analysis. In this phase, the strongest emission lines from two elements, Pb and Cu, were to be investigated separately using cathodes of different sizes and materials. In the second phase, the microcavity hollow cathode glow discharge was to be investigated as a multielement source and simultaneous determination of Pb, V and Cr was to be attempted. Chapter 5 will present the optimization procedures and results for the multielement studies, but the optimization studies for the single element phase of the project will be presented below. Where necessary, a simplex optimization procedure was followed.

Pressure, Voltage and Current

In a glow discharge operating in the abnormal regime, there is an interdependence of pressure, voltage and current. Only two of these parameters

may be varied at the same time. Because the high voltage power supply used in these experiments is a voltage-controlled power supply, the measurements of this study were made by either holding the pressure constant and varying the voltage or by holding the voltage constant and varying the pressure. Since the current could not be controlled, it was always one of the variables.

It was important to approach the optimization of the pressure, voltage and current systematically. The physical processes within the glow discharge are so complex that every element of the cathode and chamber has an effect on the stability of the discharge and the intensity of the emission signal. The optimum pressure and voltage for one particular microcavity could well be different for another one. Therefore, separate optimization studies were performed for different analytes, different cathode materials and different cathode geometries.

Four different cathode materials were evaluated: W, Ti, Al and Cu. Since tungsten is a hard metal and has a high melting point, it was hoped that it would promote sputtering of the analyte residue off the cathode surface but not be sputtered itself. If this were to happen, the emission spectrum would be free of cathode material emission lines, which could often cause severe spectral interference. Unfortunately, tungsten proved to be an inappropriate cathode material for this project. Although a very stable, brilliant discharge was able to be initiated at 600 V and 2.5 Torr, the cathode overheated almost immediately. In addition, emission from the blank electrode showed a sizeable Cu signal due to

contamination in the metal It also proved to be a poor cathode material for Pb analysis After many attempts and many adjustments, only an insignificant signal was detected, and that was for a 2 μg sample The tungsten cathode was abandoned Initial studies of the other three cathode materials looked promising, so pressure, voltage and current optimization of Ti Al and Cu microcavity hollow cathodes proceeded

The first set of optimization experiments were performed with Pb as the analyte Figures 3-4 through 3-7 show plots of the signal-to-background ratio (S/B) vs pressure at a series of constant voltages In all cases, the sample size was 100 ng of Pb in the Al microcavity hollow cathode The range of voltages was dictated by plasma stability The range of pressures was determined by simplex optimization Once the range of pressure was determined, replicate measurements (at least 3) were taken at 0 5 Torr intervals The error bars on these plots, as well as all other plots represent ± one standard deviation from the mean The results from this study indicated that the optimum voltage and pressure for Pb in the Al microcavity were 620 V and 3 Torr, respectively, resulting in a current of 42 mA

At this point, it is important to explain exactly what the signal to-background ratio represents in these plots The lead emission line that was used was 405 78 nm The Pb emission signal at this wavelength is detected by the photodiode array over a range of several diodes, with a signal maximum at a

Figure 3 4 A plot of S/B vs pressure at 560 V for 100 ng Pb in the Al microcavity

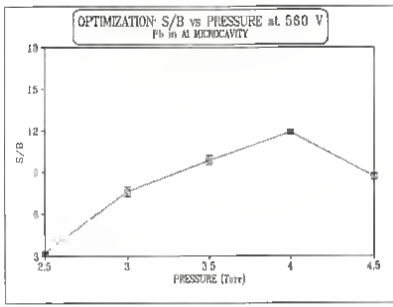
OPTIMIZATION: S/B vs PRESSURE at 560 V
Pb in Al RECTOCAVITY
S/B
PRESSURE (Torr)
2.5
3
3.5
4
4.5

Figure 3-5 A plot of S/B vs pressure at 580 V for 100 ng Pb in the Al microcavity

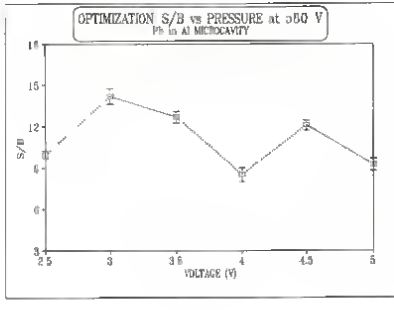
OPTIMIZATION S/B vs PRESSURE at 550 V
Pb in Al MICROCAVITY
S/B
VOLTAGE (V)
2.5
3
3.5
4
4.5
5
3
6
9
12
15
18

Figure 3-6 A plot of S/B vs pressure at 600 V for 100 ng Pb in the Al microcavity

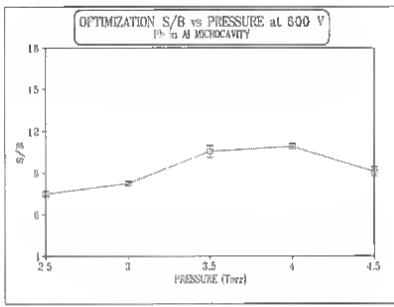
OPTIMIZATION S/B vs PRESSURE at 600 V
Pb in Al MICROCAVITY
S/B
1.8
1.5
1.2
1
2.5
3
3.5
4
4.5
PRESSURE (Torr)

Figure 3 7 A plot of S/B vs pressure at 620 V for 100 ng Pb in the Al microcavity

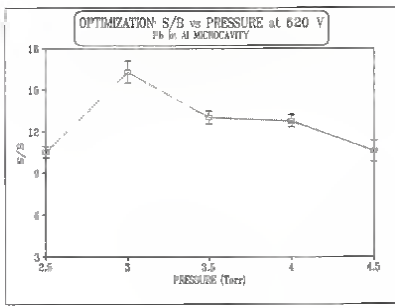
OPTIMIZATION: S/B vs PRESSURE at 620 V
Pb in Al MICROCAVITY
S/B
PRESSURE (Torr)
18
15
12
9
6
3
2.5
3
3.5
4
4.5

particular diode. As long as the wavelength reading on the spectrometer remains unchanged, the same diode will correspond to the 405.78 nm emission line each time a spectrum is taken. Once this diode had been determined, a series (usually 15) of blank measurements were taken. Each blank consisted of a volume of Barnstead water equal to the volume of Pb solution to be analyzed. The blank analysis was conducted under the same discharge conditions as the analyte. The signal for each blank at the lead diode was recorded. The average signal at the Pb diode for the 15 blank measurements was calculated. This was the signal due to the blank. Then, replicate measurements (at least 3) of Pb solution residues were taken and the average of these signals was calculated. The signal represented in the signal to-background ratio was the net signal, the average analytical signal minus the average blank signal. The background measurement was taken as the average signal of 10 diodes to either side of the Pb emission line profile. Although not shown in the optimization plots presented in this chapter, the signal-to noise ratio followed the same pattern as the signal-to-background.

The pressure and voltage were also optimized for Pb in the Cu microcavity hollow cathode for 0.7-ng samples. Figures 3-8 through 3.11 show the plots of S/B vs. pressure indicating the optimum voltage and pressure of Pb in the Cu microcavity to be 640 V at 3.5 Torr giving a current of 62 mA.

Next, a set of optimization experiments were performed for 0.8-ng samples of Pb in a standard size Al hollow cathode (5 mm dia. x 6 m deep). Figures 3-12

Figure 3-8 A plot of the S/B vs pressure at 580 V for 0 7 ng Pb in the Cu microcavity

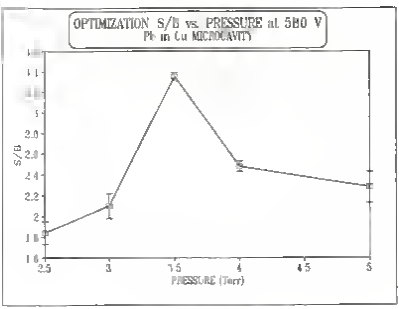
OPTIMIZATION S/B vs. PRESSURE at 580 V
Pb in Cu MICROCAVITY
S/B
2.0
2.2
2
2.5
3
3.5
4
4.5
5
PRESSURE (Torr)

Figure 3-9 A plot of the S/B vs pressure at 600 V for 0.7 ng Pb in the Cu microcavity

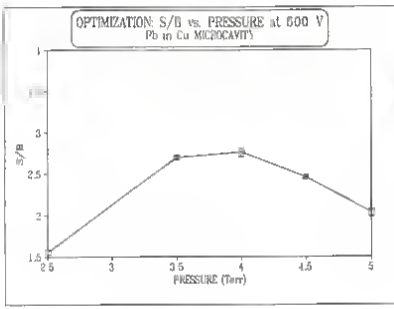
OPTIMIZATION: S/B vs. PRESSURE at 600 V
Pb in Cu MICROCAVITY
S/B
PRESSURE (Torr)
1
1.5
2
2.5
3
2.5
3
3.5
4
4.5
5

Figure 3.10. A plot of the S/B vs pressure at 620 V for 0.7 ng Pb in the Cu microcavity

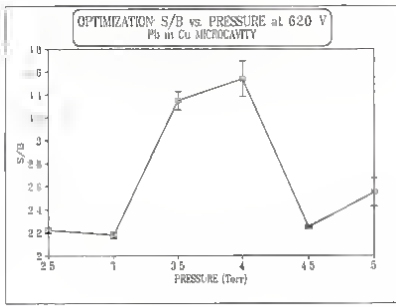
OPTIMIZATION: S/B vs. PRESSURE at 620 V
Pb in Cu MICROCAVITY
S/B
PRESSURE (Torr)
2.5
3
3.5
4
4.5
5

Figure 3.11 A plot of the S/B vs pressure at 640 V for 0.7 ng Pb in the Cu microcavity

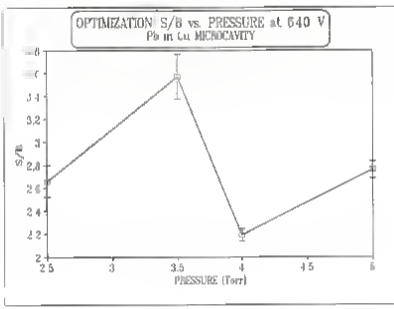
OPTIMIZATION S/B vs. PRESSURE at 640 V
Pb in Cu MICROCAVITY
S/B
3.2
3
2.8
2.6
2.4
2.2
2
2.5
3
3.5
4
4.5
5
PRESSURE (Torr)

through 3 t4 show the results of this study where the optimum voltage and pressure turned out to be 600 V at 3 Torr with a resultant current of 66 mA

Titanium was eliminated as a cathode material for Pb because it contained Pb impurities

The two cathode materials appropriate for the analysis of Cu were Al and Ti The results of the experiments to optimize the pressure, voltage and current of 200-ng samples of Cn in the Al microcavity are shown as plots (Figures 3-15 through 3-17) of S/B vs voltage at several pressnres These ptots indicate that the optimum voltage and pressnre for Cn in the Al microcavity are 600 V at 3 Torr The current was 62 mA

The same study was done for 150-ng samples of Cn in the Ti microcavity hollow cathode and resulted In the best S/B being obtained at a voltage of 680 V and a pressure of 3 5 Torr with a current of 58 mA Figures 3-18 through 3 20 show the plots of S/B vs voltage at several pressures

As can be seen from all these optimization experiments, it would not be difficult to determine compromise conditions universally applicable for the determination of all elements, perhaps 620V and 3 Torr

Chamber Pumping and Purging

Interferences from contaminants In the glow discharge chamber have been shown to have a significant impact on the fluorescence signal in a planar cathode glow discharge For example, molecular bands from species such as OH, N_2, CO

Figure 3-12. A plot of the S/B vs pressure at 580 V for 0.8 ng Pb in standard Al hollow cathode.

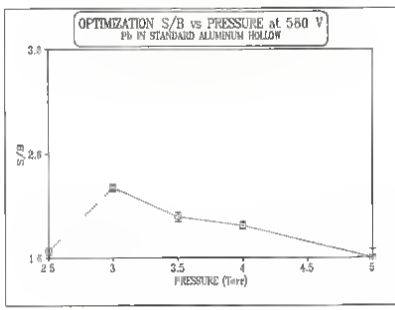
OPTIMIZATION S/B vs PRESSURE at 580 V
Pb IN STANDARD ALUMINUM HOLLOW
S/B
3.2
2.6
1.6
2.5
3
3.5
4
4.5
5
PRESSURE (Torr)

Figure 3-13 A plot of the S/B vs pressure at 600 V for 0.8 ng Pb in standard Al hollow cathode

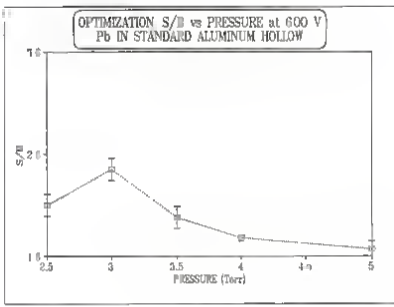
OPTIMIZATION S/B vs PRESSURE at 600 V
Pb IN STANDARD ALUMINUM HOLLOW
S/B
2.5
3
3.5
4
5
PRESSURE (Torr)

Figure 3-14 A plot of the S/B vs pressure at 620 V for 0.8 ng Pb in standard Al hollow cathode

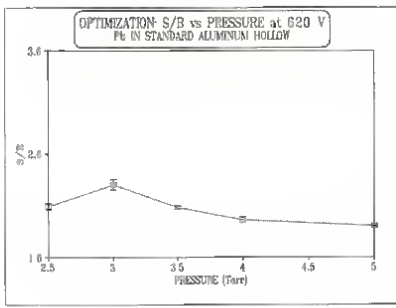
OPTIMIZATION: S/B vs PRESSURE at 620 V
Pb IN STANDARD ALUMINUM HOLLOW
3.0
2.0
1.0
S/B
2.5
3
3.5
4
4.5
5
PRESSURE (Torr)

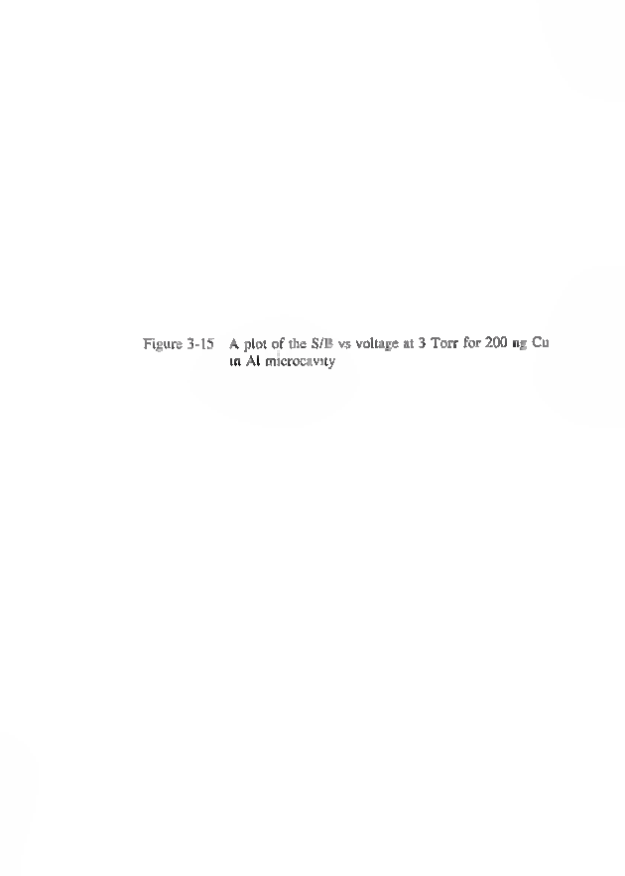

Figure 3-15 A plot of the S/B vs voltage at 3 Torr for 200 ng Cu in Al microcavity

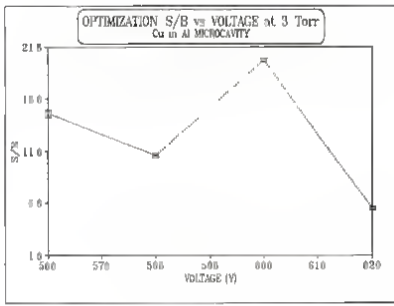
OPTIMIZATION S/B vs VOLTAGE at 3 Torr
Cu in Al MICROCAVITY
21.5
11.0
S/B
500
570
600
610
620
VOLTAGE (V)

Figure 3-16. A plot of the S/B vs voltage at 3.5 Torr for 200 ng Cu in Al microcavity

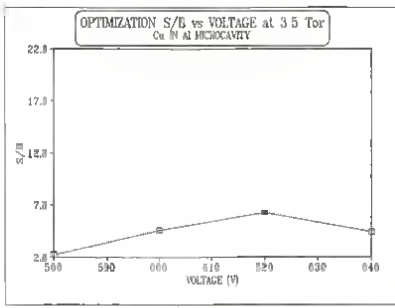
OPTIMIZATION S/B vs VOLTAGE at 3 5 Tor
Cu W Al HCHOCAVITY
22.0
17.0
12.0
7.0
2.0
S/B
500
590
000
610
620
630
640
VOLTAGE (V)

Figure 3-17 A plot of the S/B vs voltage at 4 Torr for 200 ng Cu in Al microcavity

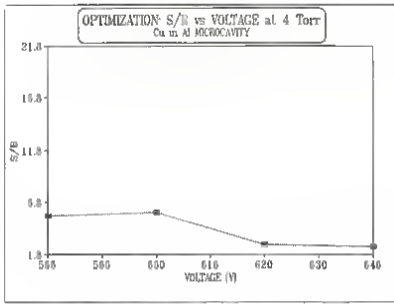
OPTIMIZATION: S/B vs VOLTAGE at 4 Torr
Cu on Al MICROCAVITY
21.8
16.8
11.8
6.8
1.8
S/B
560
580
600
620
630
640
VOLTAGE (V)

Figure 3-18 A plot of the S/B vs voltage at 3 Torr for 150 ng Cu in Ti microcavity.

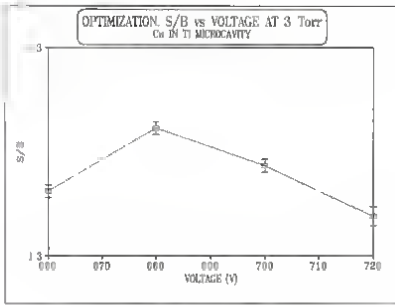
OPTIMIZATION S/B vs VOLTAGE AT 3 Torr
Cu IN Ti MICROCAVITY
S/B
3
1.3
000
070
060
000
700
710
720
VOLTAGE (V)

Figure 3-19 A plot of the S/B vs voltage at 3 5 Torr for 150 ng Cu in Ti microcavity

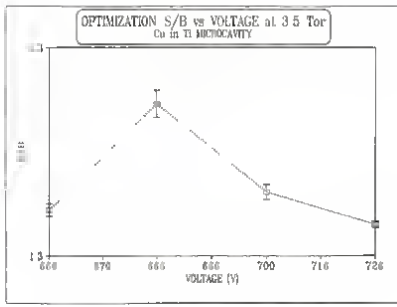
OPTIMIZATION S/B vs VOLTAGE at 3.5 Torr
Cu in Ti MICROCAVITY
1.3
670
675
680
700
715
725
VOLTAGE (V)

Figure 3-20 A plot of the S/B vs voltage at 4 Torr for 150 ng Cu in Ti microcavity

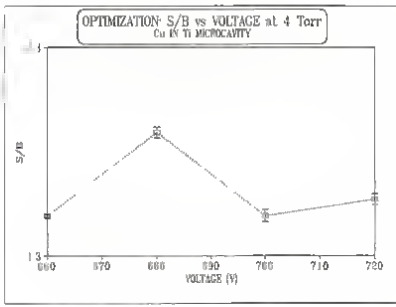
OPTIMIZATION: S/B vs VOLTAGE at 4 Torr
Cu IN Ti MICROCAVITY
S/B
VOLTAGE (V)
660
670
680
690
700
710
720

and CO_2 can degrade the analytical spectrum dramatically. Another problem that occurs with atmospheric contamination in a low pressure discharge is oxide formation, which reduces the atom number density and emission intensity.

One method that has been successful in reducing or eliminating atmospheric contamination is pumping and purging the glow discharge chamber. A study conducted previously in our laboratory indicated that the best fluorescence signal-to-noise ratio was obtained by twice evacuating the chamber to a millitorr and introducing enough argon to bring the chamber to atmospheric pressure after each evacuation. The final pressure could then be set.

In order to determine if this procedure was necessary with the microcavity hollow cathode glow discharge emission system, a study was performed which examined the relationship between the signal-to-background ratio and the number of times the chamber was pumped down. The study was done for 10-ng samples of Pb in the Al microcavity. As can be seen in Figure 3.21, there was no significant difference in S/B indicating that atmospheric contamination was not a problem in glow discharge emission.

Sample Drying Time

Another parameter to be evaluated was the sample drying time. Almost every study involving the analysis of solution residues in a hollow cathode glow discharge system reports the same drying procedure. In most previous studies, the

Figure 3-21 A plot of S/B vs purge cycles for 10 ng Pb in Al microcavity

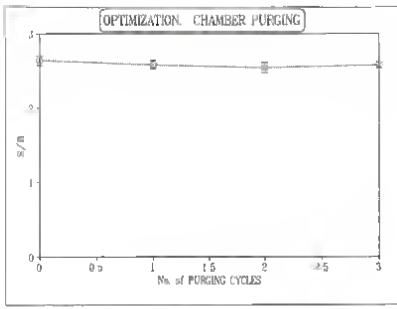
OPTIMIZATION. CHAMBER PURGING
S/N
0
1
2
3
0
0.5
1
1.5
2
2.5
3
No. of PURGING CYCLES

sample is dried onto the cathode by placing the hollow cathode containing the solution under an infrared lamp until it is dry, anywhere from 3 to 10 minutes, depending on the size of the cavity and the size of the sample. Previous reports indicate that the sample should be completely dried to avoid contamination from water.

Initially, this procedure was followed. However, because the sample size at that time was 2 μL, the sample more than half-filled the very small microcavity hollow. It required 10 minutes under the infrared lamp to dry. Problems arose when the pyrex cathodes would heat up excessively and either warp or crack, rendering them unusable. It was then decided to let the cathodes just air dry. This also presented problems. It took over 30 minutes for the sample to dry, which allowed time for an oxide layer to form on the inside of the cavity. When this happened it was very difficult to initiate the discharge. It was finally decided to dry the cathodes under a gentle stream of dry nitrogen for 10 minutes. This drying procedure worked well. The solution dried onto the cathode and the discharge was easy to light and maintain.

As often happens in research, the importance of drying time was happened upon quite by accident. One day, in making a "quick-and-dirty" measurement on a sample that had only been drying for 1-2 minutes, the signal was, unexpectedly, a good three times that of any previous measurement of comparable mass. It was clear this phenomenon had to be investigated. A study of the effect of sample

drying time on S/B was immediately performed. The results are shown in Figure 3-22, which plots the S/B vs the sample drying time for 400 ng Pb in the Al microcavity. From this plot, it is clear that the best signal-to-background ratio is achieved with only a minimum of drying time. Perhaps, it is the case that oxides form no matter what drying method is used, and that a larger population of free atoms is attainable when solutions are not thoroughly dried. A similar study was done when nanoliter sized samples began to be used. This study indicated that the best signal-to-background ratio was achieved when the sample was not dried at all.

Slit Width

A very simple optimization study of the S/B vs the entrance slit width of the monochromator was carried out. Figure 3-23 shows the plot of S/B vs. slit width for 200 ng Pb in the Al microcavity. The results indicate that the optimum slit width is 10 μm. This study was also done for 10 ng Cu in the Al microcavity with similar results.

Cathode Preconditioning

Several authors have studied the effects of preconditioning the hollow cathode to maximize the emission signal and improve precision.[87,93,116] Careful machining of the hollow cathode results in a cylinder with a flat bottom. These studies have shown that the sputtering process reshapes the hollow cathode from the original flat bottom to a spherical cavity. The walls of the hollow cathode also undergo a change. While the bottom is becoming spherical, there is a position

Figure 3.22 A plot of S/B vs drying time

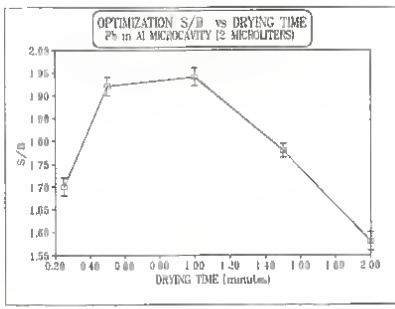
OPTIMIZATION S/B vs DRYING TIME
Pb in Al MICROCAVITY (2 MICROLITERS)
S/B
2.05
1.95
1.90
1.85
1.80
1.75
1.70
1.65
1.60
1.55
0.20
0.40
0.60
0.80
1.00
1.20
1.40
1.60
1.80
2.00
DRYING TIME (minutes)

Figure 3.23 A plot of S/B vs slit width

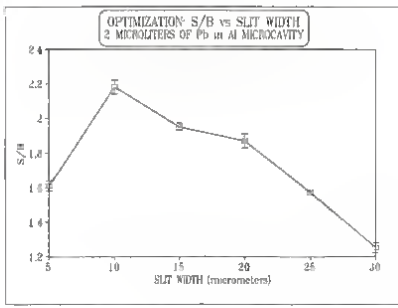
OPTIMIZATION: S/B vs SLIT WIDTH
2 MICROLITERS OF Pb in Al MICROCAVITY
S/B
2.4
2.2
2
1.8
1.6
1.4
1.2
5
10
15
20
25
30
SLIT WIDTH (micrometers)

along the wall which begins to constrict. Figure 3-24 illustrates this process. It has been shown that the discharge is most stable when the cathode achieves this shape. In a recent study on cathode aging, Williams[116] claimed he achieved complete aging of a Cu microcavity after 350 ± 5 discharges.

This seemed a valuable study to take note of, and it was decided that a similar aging procedure would be followed for the microcavities in this project. To avoid overheating the cathodes, they were aged for 500 5 s discharges over a period of a few hours. Although this was presumed to be sufficient preconditioning, it was not. It was observed that after more than 1000 discharges beyond those required for aging, the Al microcavity hollow cathode suddenly changed. The current to the discharge decreased by 50-70% for the same applied voltage and the same pressure. More importantly however, was the fact that the sensitivity increased dramatically. In reviewing Williams' study, it was clear that although a spherical bottom had been formed after 350 ± 5 discharges, the constriction at the wall had not formed. Pictures of his microcavities show that even after 1500 ± 5 discharges the constriction was just beginning to be formed. White[91] has reported that optimum performance is reached when the ratio of the diameter of the aperture formed by the constriction to the diameter of the spherical bottom is 0.25. The abrupt change in the performance of the Al microcavity hollow cathode may have come at the point where this particular hollow cathode achieved dimensional stability. For whatever reason, the best results (to be presented in Chapter 4) were obtained after the change took place.

Figure 3 24 An illustration of cathode aging


NEW
CATHODE
PARTIALLY AGED
CATHODE
FULLY AGED
CATHODE

CHAPTER 4

SINGLE ELEMENT DETERMINATION OF COPPER AND LEAD IN NANOSAMPLE SOLUTION RESIDUES BY MICROCAVITY HOLLOW CATHODE GLOW DISCHARGE

Evalnation of the microcavity hollow cathode glow discharge as a source for simultaneous multielement analysis of discrete nanoliter samples was carried out in two phases Each phase was designed to answer a question First of all, would the microcavity hollow cathode glow discharge prove to be a good source for ultratrace analysis of discrete nanoliter samples? Secondly, would this source be applicable to multielement determination? This chapter focuses on a series of experiments designed to answer the first qnestion

Two elements, Cu and Pb were chosen for these analyses. Each element was evaluated individually using its strongest emission line - 324 7 nm for Cu and 405 78 nm for Pb

Experimental

The experimental setup used in the single element analysis experiments was described in Chapter 3 Calibrated neutral density filters were used for all optimized measurements In addition, a 10-nm bandpass interference filter centered at 320 nm was used for the Cu determinations

Sample Preparation

This study required minimal sample preparation. Solutions of various concentrations of Cu and Pb were prepared by appropriate dilutions of 1000 ppm research grade standard solutions (Fisher Scientific) with Barnstead (doubly deionized) water. Volumetric flasks used in these preparations were thoroughly cleaned and soaked in concentrated nitric acid.

Delivery of the sample solution onto the cathode was accomplished with the use of a micropipet. Initially, 2 μL samples were used and were delivered with a calibrated 2 μL Eppendorf pipet that had an accuracy rating of 0.3% and a precision of 0.2%. Disposable pipet tips were used in all cases. Subsequently, nanoliter samples were delivered by a newly factory calibrated Rainin micropipet, Model P-2 "Pipetman," using disposable metal-free pipet tips. This particular micropipet was calibrated to deliver volumes from 1 nL to 1 μL with precisions ranging from 14% for volumes below 50 nL to 0.3% for volumes above 500 nL. The smallest volume used in this study was 50 nL.

Experimental Procedure

Over a period of several months and through much trial and error, an experimental procedure was developed which was consistent and effective. Firstly, the spectrometer wavelength selector was set to the appropriate wavelength. Initial spectra were taken 1) with the spectrometer slits closed, 2) with the spectrometer slits opened and the room lights off and 3) with the slits opened and the room

lights on. Analyses of these spectra gave an indication of the contribution of each set of conditions to the spectral backgronnd. All cathodes ware cleaned with 5% nitric acid prior to a day's work. The copper cathodes were soaked for about 2 minnies whila the Al and Ti cathodes needed to soak overnight. This ensured a clean surface, which was verified by preburning the dry, clean cathode and analyzing the resnltant spectrum. A series of blanks were run next. This consisted of ten to fifteen individual spectra of Barnstead water in whichever cathode was to be used for analytical determinations. A particular volume of Barnstead water was deposited onto the cathode bottom and the cathode was inserted into the glow discharge chamber. The chamber was evacuated to about 1 mTorr aod set to the appropriate pressnre as monitored by a capacitance manometer. The voltage was then set.

The data acquisition began prior to ignition of the discharge in order to record the baseline with the discharge off. The switch was then thrown and the discharge initiated. The ST 120 software, which was nsed for data acquisition and processing, allowed great flexibility in setting the parameters of data acqnisition. The signal could be integrated over a period of time or a number of scans with the same integration time could be averaged or a combination of the two could be selected. A previous study performed in onr lab indicated that the optimum signal-to noise was achieved by integrating signals for longer periods of time rather than averaging spectra. The integration time for most of these experiments was set to

1 s, which represented integration over 30, 0 033-s scans, and, subsequently, two spectra were averaged The ST t20 software also enabled the behavior of the analytical signal to be observed over time Either a single spectrum or a 3-D spectrum could be generated. Since this work was based on discrete sampling, the signal was transient and the 3-D plot was very useful in helping to determine if the entire sample had been sputtered off the cathode Figure 4-1 shows an example of the temporal behavior of an analytical signal

Once the data had been acquired the discharge was manually switched off Having acquired the data for the blank signals, the analyte samples were then determined in the same manner as the blank samples had been determined. The one difference was the necessity to perform cleansing afterburns of the cathode to make sure any analyte that had redeposited on the cathode surface was sputtered off In the case of Pb, this could take as long as fifteen 3-s discharges In all cases, care had to be taken so as not to overheat the cathode The appropriate spectra were saved on floppy disk for further analysis

Determination of Copper

Through a series of experiments it was determined that Al and Ti cathodes should be used in the determination of Cu The emission wavelength chosen for the analysis was 324 754 nm The Al microcavity proved to be the best cathode, providing a stable, reproducible discharge and a limit of detection superior to previous glow discharge emission work. Figure 4-2 shows the analytical

Figure 4-1 An emission spectrum of Pb showing the temporal behavior of the signal

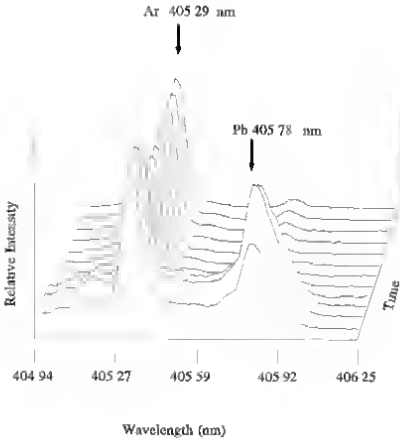
Ar 405 29 nm
Pb 405 78 nm
Relative Intensity
Time
404 94
405 27
405 59
405 92
406 25
Wavelength (nm)

Figure 4-2 Calibration curve of Cu in the Al microcavity at 324.7 nm

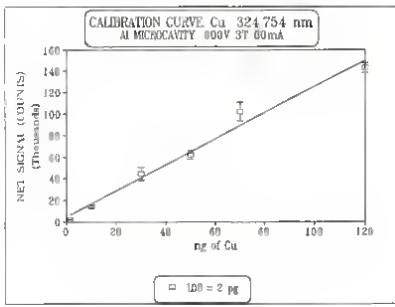
CALIBRATION CURVE Cu 324.754 nm
Al MICROCAVITY 600V 3T 60mA
NET SIGNAL (COUNTS)
(Thousands)
ng of Cu
LOD = 2 pg

calibration curve of Cu in the Al microcavity. This calibration curve, as well as all others presented in this chapter, was generated using peak heights. The net signal(the Y-axis of the calibration curves) represents the analytical signal less the signal due to the blank and less the baseline signal. The baseline signal was determined as the average intensity of 10 diodes on either side of the emission line away from the wings of the peak. The best fit line was generated by a linear least squares regression analysis.

The limits of detection in these analyses were determined using the 3σ method, with σ representing either the standard deviation of the background or the standard deviation of the blank. The method most often reported in the glow discharge literature uses the $3\sigma_{bk}$ method. For the analysis of Cu in the Al microcavity hollow cathode the limit of detection based on $3\sigma_{bk}$ was calculated to be 2 pg. The more conservative approach, $3\sigma_{bl}$, gave a limit of detection of 15 pg. The correlation coefficient, r^2, was 0.982 and the log-log slope was 0.992. This was based on experiments in which increasing volumes of the same concentration of solution were determined. The same process was repeated by sampling equal volumes of differing concentrations. There were no significant differences in the figures of merit for either method of sample delivery. The precision, based on at least 3 replicate measurements, of the Cu analysis ranged from 11% to 18% RSD and the calibration curve was linear over 2-3 orders of magnitude.

Cu was also determined using a Ti microcavity hollow cathode. These experiments were fraught with difficulties. The Ti cathode proved extremely temperamental. It was very difficult to initiate a stable plasma. The cathode would also heat up very rapidly. It took a monster effort to obtain any reasonable analytical data. Figure 4-3 shows the calibration curve for Cu in the Ti microcavity. The limit of detection based on $3\sigma_{bk}$ was, however, a respectable 77 pg. The limit of detection based on $3\sigma_{sd}$ was 470 pg. The precision ranged from 2% to 16% RSD. The value of r^2 was 0.976 and the log-log slope was 0.977.

In order to contrast the results obtained using the microcavity with those that would be obtained using a standard size hollow cathode, Cu was also determined in an Al standard hollow cathode (5 mm dia.). The calibration curve is presented in Figure 4-4. The limit of detection for $3\sigma_{bk}$ was 1 ng and for $3\sigma_{sd}$ was 7 ng. In this case the r^2 was 0.994 and the log-log slope was 1.087. The precision ranged from 5% to 13% RSD.

Determination of Lead

Through another series of experiments, it was determined that Cu and Al microcavity hollow cathodes would be used for the determination of Pb. The emission wavelength chosen for the analysis was 405.78 nm. Here, again, the Al microcavity hollow cathode proved to be the best cathode. A stable, reproducible discharge was easy to initiate and to maintain. The cathode was not subject to

Figure 4-3 Calibration curve of Cu in the Ti microcavity at 324.7 nm

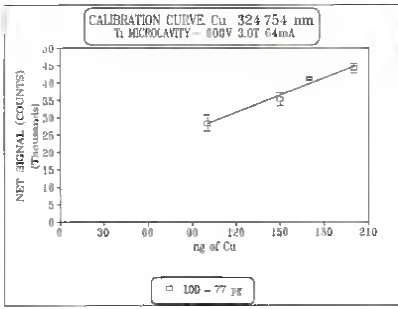
CALIBRATION CURVE Cu 324 754 nm
Ti MICROCAVITY – 800V 3.0T 64mA
NET SIGNAL (COUNTS)
(Thousands)
ng of Cu
0
5
10
15
20
25
30
35
40
45
50
0
30
60
90
120
150
180
210
100 – 77 pg

Figure 4-4 Calibration curve of Cu in the standard Al hollow at 324 7 nm

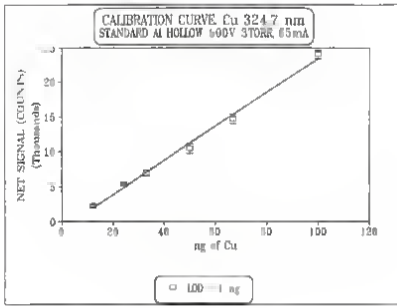
CALIBRATION CURVE Cu 324.7 nm
STANDARD AI HOLLOW 500V 3TORR 65mA
NET SIGNAL (COUNTS)
(Thousands)
0
5
10
15
20
0
20
40
60
80
100
120
ng of Cu
LOD = 1 ng

undo heating problems. The limits of detection obtained for Pb using the Al microcavity were far superior to previous glow discharge emission work and, in fact, rivaled glow discharge fluorescence.

Figure 4-5 shows the analytical calibration curve for Pb in the Al microcavity. As in the case of the copper analysis, comparable detection limits were obtained for sampling different volumes of the same concentration of solution and for sampling equal volumes of different concentrations. The calibration curve was reproducible from day to day and from one Al microcavity to another of equal age. The detection limit for Pb in the Al microcavity hollow cathode was 36 fg using the $3\sigma_{bk}$ method and 140 fg using the $3\sigma_{bl}$ method. The r^2 value was 0.977 and the log-log slope was 1.102. The precision ranged from 7% to 22% RSD.

Pb was also determined in the Cu microcavity hollow cathode. Figure 4-6 shows the analytical calibration curve for Pb in the Cu microcavity. The $3\sigma_{bk}$ limit of detection was calculated to be 1.8 pg and the $3\sigma_{bl}$ limit of detection was 172 pg. Here, the r^2 was 0.992 and the log-log slope was 1.142. The precision ranged from 7% to 15 % RSD.

In order to show a comparison of the limits of detection of Pb in the Al microcavity and the Al standard hollow cathode, Pb was determined in a standard (5 mm dia) Al hollow cathode. The calibration curve is presented in Figure 4-7. The limit of detection based on $3\sigma_{bk}$ was 14 ng and the $3\sigma_{bl}$ detection limit was 26 ng. The r^2 value was 0.986 and the log-log slope was 1.346.

Figure 4-5 Calibration curve of Pb in the Al microcavity at 405.78 nm

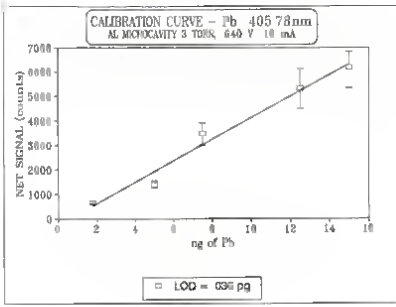
CALIBRATION CURVE – Pb 405.78nm
AL MICROCAVITY 3 TORR, 640 V 10 mA
NET SIGNAL (counts)
7000
6000
5000
4000
3000
2000
1000
0
0
2
4
6
8
10
12
14
16
ng of Pb
LOD = 636 pg

Figure 4-6 Calibration curve of Pb in the Cu microcavity at 405 78 nm

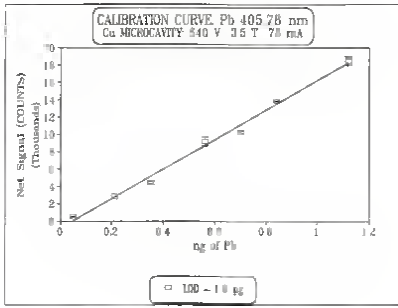
CALIBRATION CURVE Pb 405 78 nm
Cu MICROCAVITY 540 V 35 T 75 mA
Net Signal (COUNTS)
(Thousands)
ng of Pb
LOD ~ 1 0 pg

Figure 4.7 Calibration curve of Pb in the standard Al hollow at 405.78 nm

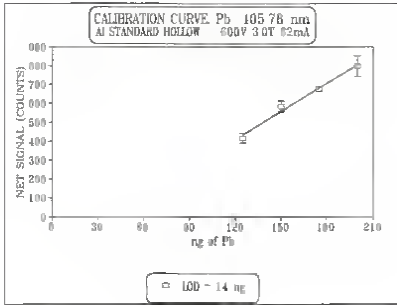
CALIBRATION CURVE Pb 405.78 nm
AI STANDARD HOLLOW 600V 3.0Y 02mA
NET SIGNAL (COUNTS)
0
100
200
300
400
500
600
700
800
900
0
30
60
90
120
150
180
210
ng of Pb
LOD ~ 14 ng

Effect of Na on the Analytical Signal

In order to determine if there was any effect on the analytical signal from easily ionizable elements, a series of experiments were performed to ascertain what, if any, concentration of Na added to the analyte solution would suppress the analytical signal. Figure 4-8 shows a log-log plot of the S/B of Pb vs the concentration of added Na. As can be seen from this plot, there is an effect on the analytical signal. The suppression of the signal begins when the mass of Na is 100 times that of the analyte but is really pronounced when the mass of Na is greater than 300 times that of the analyte.

Limiting Noises

No discussion of a new technique would be complete without a close look at the limiting noises of the system. Figure 4-9 is a graph which characterizes the different analyte cathode combinations based on the major sources of noise. These noises can be categorized into three areas – dark current, background emission with a clean cathode and background emission when analyte is present. In most cases, the major contributor to the noise of the system is the background emission from the blank cathode with a small contribution from the background emission when analyte is present. However, in the case of Pb in the Al microcavity hollow cathode, there is a difference. Notice that the major contributor to noise is no longer background emission from the blank but is background emission from the analytical signal. This shift in the relative contribution of the noises may help

Figure 4-8 Log-log plot of S/B vs concentration of Na showing the effect of Na on the Pb analytical signal in the Al microcavity at 405 78 nm

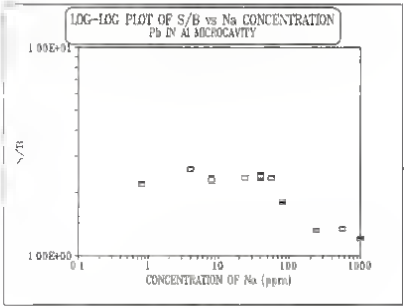
LOG-LOG PLOT OF S/B vs Na CONCENTRATION
Pb IN Al MICROCAVITY
1.00E+01
1.00E+00
S/B
0.1
1
10
100
1000
CONCENTRATION OF Na (ppm)

Figure 4 9 Graph showing the limiting noises for each analyte cathode combination The signal intensities are normalized for the total noise in the worst case (Pb in the Cu microcavity)

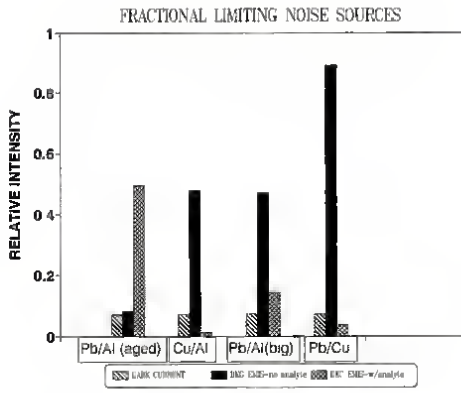
FRACTIONAL LIMITING NOISE SOURCES
RELATIVE INTENSITY
1
0.8
0.6
0.4
0.2
0
Pb/Al (aged)
Cu/Al
Pb/Al(big)
Pb/Cu
DARK CURRENT
IMD EMF-no analyte
IEC EMF-w/analyte

explain the extraordinary results using a fully aged cathode. White[93] claimed that once dimensional stability was reached the dimensions of the hollow remain constant and an equilibrium between sputtering and redeposition was reached. In such a stable configuration, the contribution of sputtering of cathode material is decreased. The sample deposited on the cathode may be sputtered preferentially, thus explaining the increased contribution of the noise from analyte background emission. Even though the total noise in cases one and two (Pb in the aged Al microcavity and Cu in the newer Al microcavity) are comparable, the S/N is much greater in the case of the aged hollow. For a 15 pg sample of Pb in the aged Al microcavity, the S/N is 1240. For a 50 pg sample of Cu in a newer Al microcavity the S/N is 50. This represents a dramatic difference, however a better comparison would be to look at the S/N of Pb in a newer Al microcavity and in the fully aged Al microcavity. Experiments performed to analyze Pb in the Al microcavity before it had been completely aged resulted in a S/N, for a 15 pg sample, of 537. A better than twofold increase in signal-to noise is achieved upon dimensional stability of the cavity.

Determination of Pb in Real Samples

A complete evaluation of the microcavity hollow cathode as a source for trace and ultratrace analysis must include the evalnation of the accuracy of the method. The NIST standard reference material #1643b "Trace Elements in Water"

was chosen as the standard with which to perform this evaluation The certified concentration of Pb in this standard is 24 1 ± 0 07 ppb

It was decided that the reference standard would be analyzed for Pb in both the Al and Cu microcavity hollow cathodes The results were accurate within experimental error Four replicate measurements of the standard reference material were taken and the Pb emission in the Cu microcavity hollow cathode was analyzed The results of these measurements determined the concentration of Pb to be 22.3 ± 3 4 ppb Three replicate measurements of this same standard reference material were taken using the Al microcavity hollow cathode The concentration of Pb in the standard reference material with this cathode was 26 1 ± 3.8 ppb

Discussion

The results of these studies have been very promising The microcavity hollow cathode glow discharge has been shown to be a good source for trace and ultratrace analysis for discrete nanoliter samples With a fully aged Al microcavity femtogram detection limits are achievable for Pb. Table 4-1 compares the results of these experiments with other glow discharge work Also included in Table 4-1 are results of Pb and Cu analysis using other techniques

Table 4-1 Absolute Detection Limits for Aqueous Cu and Pb Samples

	Cu (pg)		Pb (pg)	
THIS WORK	$3\sigma_{bk}$	$3\sigma_{bl}$	$3\sigma_{bk}$	$3\sigma_{bl}$
Ti microcavity	77	470		
Cu microcavity			1 8	172
Al microcavity	2	15	0 036	0 140
Al standard hollow	1000	7000	14000	26000
OTHER GD WORK				
GD Emission (standard)	40[45]		900[106]	
GD LEAFS			2[14]	
GD - AAS (pulsed)	3[117]			
GD - Magnetron AES	8[45]		40000[45]	
OTHER TECHNIQUES				
Cu Spark			5000[118]	
dc Arc	30000[118]		100000[118]	
ETA AAS	2[119]		7.5×10^{-4} [119]	
ICP AES (microsampling)	51[120]		450[120]	

In addition, experimental conditions can be set such that a stable discharge, easy to initiate and easy to maintain can routinely be achieved Some other attributes of the microcavity hollow cathode include the lack of memory effects and long lifetime It was found in these experiments that the surface could be cleaned by repeated sputtering until the baseline returned to its original value It was also found that, if properly cooled, the cathodes were very hardy and long-lasting From this study, it is hard to predict the exact lifetime but the oldest cathode has undergone over 1500 discharges and still gives good results

CHAPTER 5
SIMULTANEOUS MULTIELEMENT DETERMINATION OF DISCRETE MICROSAMPLE SOLUTION RESIDUES BY MICROCAVITY HOLLOW CATHODE GLOW DISCHARGE EMISSION

This chapter will focus on experiments designed to determine if microcavity hollow cathode glow discharge emission is applicable to simultaneous multielement analysis

Since the detection system used in these studies was a photodiode array with a 20 nm window, the process of finding a group of elements with emission lines sufficiently intense, easily resolvable from background emission lines and located within a 20 nm span was a tedious one After many preliminary experiments, it was decided to focus on three elements - Cr at 359 35 nm, Pb at 363 96 nm and 368 35 nm, and V at 370 36 nm All of these emission lines were of moderate intensity

Experimental

The experimental setup used in the simultaneous multielement analysis study was described in Chapter 3 The spectrometer was set at 368 77 nm which gave a spectral window ranging from 358 77 nm to 378 77 nm Calibrated neutral density filters were used in all determinations In addition a UG5 filter was placed in front of the aperture to block visible light from reaching the detector

The photodiode array used in this particular phase of the project was the Princeton Instruments ST-110.

Sample Preparation

This study also required minimal sample preparation. Solutions of various concentrations of the three analytes were prepared from stock solutions (Fisher Scientific) with Barnstead water.

Delivery of the sample volumes onto the microcavity cathode surface was accomplished with a calibrated 2 μL Eppendorf pipet which had an accuracy of 0.3% and a precision of 0.2%. Disposable pipet tips were used for all sampling. At the time of this study, the nanoliter pipet was being repaired and recalibrated and was not available for use. All sample volumes for the multielement analysis, therefore, were 2 μL.

Experimental Procedure

The experimental procedure used during this phase of the project was similar to that described in Chapter 4, with two exceptions. Firstly, because the sample volumes delivered into the cathode cavity were 2 μL, a one minute drying step was added to the procedure. Secondly, the spectra generated with the ST-110 photodiode array were all one-dimensional, and so the signal could not be monitored as a function of time. The more sophisticated ST-120 photodiode array was unavailable at the time of this study. The integration times were optimized for this setup.

Optimization

The optimization procedure for this study was much less rigorous than for the single element determination study outlined in Chapter 4. The purpose of this study was to show that simultaneous multielement determination could be achieved with this source, which, under the compromised experimental conditions, meant that the best detection limits would not be achieved. Some of the optimizations performed for this phase are presented in Figures 5-1 through 5-6. For Pb, the optimum voltage and pressure were 560 V and 3 Torr, respectively. For Cr, the optimum voltage and pressure were 580 V and 3 Torr. Finally, for V, the optimum voltage and pressure were 560 V and 3 Torr. Having determined the optimum voltage and pressure for the three analytes individually, it was decided that for the simultaneous multielement determination, the compromise voltage and pressure would be set to 560 V and 3 Torr.

Results

Figure 5-7 demonstrates that simultaneous multielement determination of discrete nanosamples of solution residues of Cr, Pb and V was achieved. Since this work was performed under compromise conditions, using only moderately intense emission lines, determining limits of detection would be of little value. Once it was proved that the microcavity hollow cathode was amenable to multielement analysis, it could be coupled to a detection system which would allow for the analysis of many (50-60) elements at one time using the most intense

Figure 5-1 A plot of S/B vs Voltage at 3 Torr for Pb in the Al microcavity at 368.35

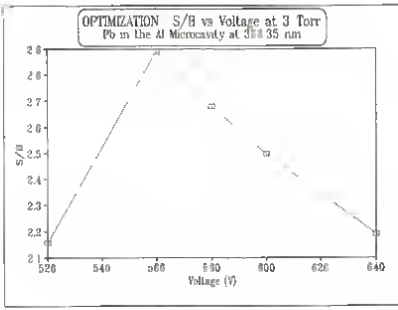
OPTIMIZATION S/B vs Voltage at 3 Torr
Pb in the Al Microcavity at 368.35 nm
S/B
2.8
2.6
2.7
2.6
2.5
2.4
2.3
2.2
2.1
520
540
560
580
600
620
640
Voltage (V)

Figure 5 2 A plot of S/B vs Pressure for Pb in the Al microcavity at 368 35 nm

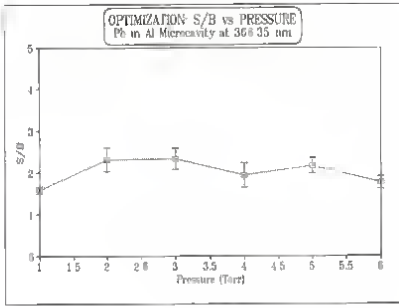
OPTIMIZATION: S/B vs PRESSURE
Pb in Al Microcavity at 360 35 nm
S/B
5
4
3
2
1
0
1
1.5
2
2.5
3
3.5
4
4.5
5
5.5
6
Pressure (Torr)

Figure 5 3 A plot of S/B vs Voltage for V in the Al microcavity at 370 36 nm

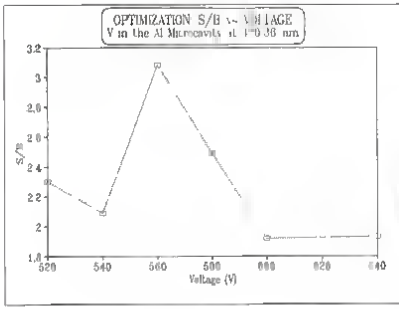
OPTIMIZATION S/B vs VOLTAGE
V in the Al Microcavity at l=0.36 mm
S/B
3.2
3
2.8
2.6
2.4
2.2
2
1.8
520
540
560
580
600
620
640
Voltage (V)

Figure 5 4 A plot of S/B vs Pressure for V in the Al microcavity at 370 36 nm

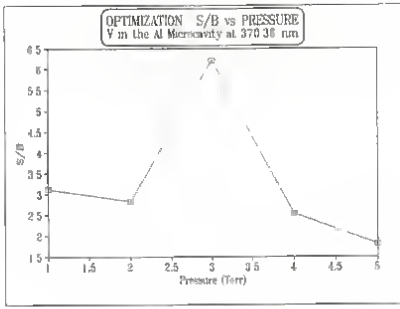
OPTIMIZATION S/B vs PRESSURE
V in the Al Microcavity at 370 38 nm
S/B
Pressure (Torr)
6 5
6
5 5
5
4 5
4
3 5
3
2 5
2
1 5
1
1 5
2
2 5
3
3 5
4
4 5
5

Figure 5-5 A plot of S/B vs Voltage for Cr in the Al microcavity at 359.35 nm

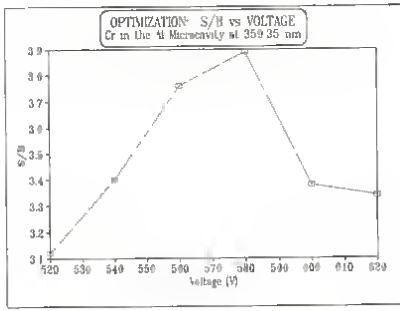
OPTIMIZATION S/B vs VOLTAGE
Cr in the Al Microanalyt at 359.35 nm
S/B
3.9
3.8
3.7
3.6
3.5
3.4
3.3
3.2
3.1
520
530
540
550
560
570
580
590
600
610
620
Voltage (V)

Figure 5-6 A plot of S/B vs Pressure for Cr in the Al microcavity at 359 35 nm

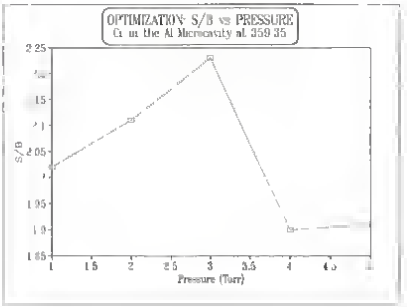
OPTIMIZATION: S/B vs PRESSURE
Cu on the Al Microcavity at 359.35
S/B
Pressure (Torr)
2.25
2.1
2.05
2
1.95
1.9
1.85
1
1.5
2
2.5
3
3.5
4
4.5

Figure 5·7 A spectrum showing simultaneous multielement determination of Cr, Pb and V

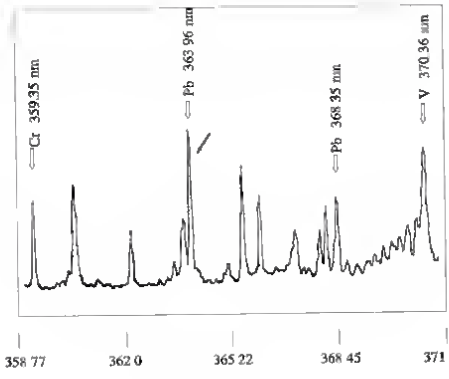
⇐Cr 359.35 nm
⇐Pb 363.96 nm
⇐Pb 368.35 nm
⇐V 370.36 nm
358.77
362.0
365.22
368.45
371.67
Wavelength (nm)

emission line for each element. Unnecessary as it seemed, it was decided that the detection limit for Pb at this wavelength would be determined and compared to the detection limit presented in the previous chapter for the strongest emission line. A calibration curve was generated and is presented in Figure 5-5. The limit of detection based on the $3\sigma_{bk}$ method was 260 pg. Even though it was some 10000 times higher than the 36 fg detection limit achieved at the 405.78 nm emission line, it is nevertheless impressive. Amazingly enough, it is superior to Becerra's[166] glow discharge emission work, in which he reported a detection limit of 900 pg for Pb using a standard hollow cathode and measuring at the very strong 283.3 resonance line.

Discussion

The findings of this study indicate that the microcavity hollow cathode glow discharge shows promise as a simultaneous multielement source. Even under compromise conditions, the detection limits are excellent. This study, however, was not without its problems. Vanadium proved to be a tricky element to analyze. The discharge with a V sample would sometimes fail to ignite immediately. It was found that in order to obtain a reproducible discharge when V was present, the cathode had to be thoroughly cleaned before each run. Once the vanadium discharge was initiated, however, it was very stable.

Figure 5 8 A calibration curve of Pb in the Al microcavity at 368 35 nm

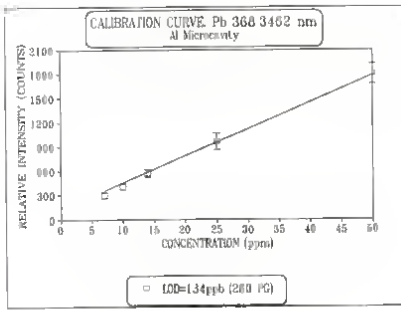
CALIBRATION CURVE Pb 368.3462 nm
Al Microcavity
RELATIVE INTENSITY (COUNTS)
2100
1800
1500
1200
900
600
300
0
0
5
10
15
20
25
30
35
40
45
50
CONCENTRATION (ppm)
LOD=1.34ppb (280 PG)

During this study alternative discharge gases were tried out, with poor results Helium gave a very quiet, stable discharge, but its sputtering efficiency was so low, it could not be used for analysis Neon, on the other hand, allowed for greater sputtering, but presented too many interfering lines in the spectral region

CHAPTER 6
SUMMARY, CONCLUSIONS AND FUTURE WORK

The results presented in Chapters 4 and 5 give evidence to the assertion that the microcavity hollow cathode glow discharge emission system is applicable to simultaneous multielament analysis of discrete microsamples and nanosamples of solution residues. When analyzing the strongest emission line for each element, it is an excellent source for trace and ultratrace determinations. As a signal boosting technique, the microcavity is certainly successful.

The limits of detection presented in Chapter 4 were superior to the limits of detection reported from previous glow discharge emission work, as well as many other techniques. The Pb detection limit was especially impressive with a 3-4 order of magnitude improvement over previous glow discharge emission work and a 2 order of magnitude improvement over glow discharge laser excited atomic fluorescence work.

During the course of this project, it was unexpectedly discovered that sample drying time was an important parameter to optimize. This had not previously been discussed in the literature. It was also discovered that complete aging of the cathode resulted in dimensional stability and was critical for very low detection limits.

Although this work demonstrated that coupling the microcavity hollow cathode glow discharge with a photodiode array offered the potential for simultaneous multielement analysis, it could only be obtained if the analyte emission lines were within 20 nm of each other. This is a significant drawback to the system presented here. A way to overcome this disadvantage can be suggested. If the current monochromator and photodiode array were replaced with a direct reader or an echelle spectrometer and a CCD detector, 50 or 60 elements could be detected simultaneously using each element's strongest emission line. Since the source has been proven to be so effective, this system need not be limited by the detector. Such a combination as has just been suggested could prove to be a very powerful multielement technique.

Any future work on this project should focus on improving the precision of the technique. A current controlled power supply would offer a vast improvement in this regard. A more precise sampling technique for samples less than 50 mL could also improve the precision. In addition to these two suggestions, it might be important to devise a more efficient cathode cooling system. Improvements in signal output might be accomplished by using a mixture of noble gases for the discharge gas, for example, Ar/He. Signal output could also be improved by coupling the microcavity with another signal boosting technique such as a microwave source or an rf source.

In any event, this work has laid a solid foundation for further investigation into a very interesting and promising technique.

REFERENCES

1 R. Mavrideanu, *J. Res. Nat. Bur. Stds.* **89**, 143 (1984).

2 S. Caroli, *Progr. Anal. At. Spectrosc.*, **6**, 253 (1983).

3 P. J. Slevin and W. W. Harrison, *Appl. Spectrosc. Rev.*, **10**, 201 (1975).

4 N. P. Ferreira, J. A. Strauss and H. G. C. Human, *Spectrochim. Acta*, **38B**, 899 (1983).

5 M. E. Pillow, *Spectrochim. Acta*, **36B**, 821 (1981).

6 N. P. Ferreira and H. G. C. Human, *Spectrochim. Acta*, **36B**, 215 (1980).

7 K. R. Hess and R. K. Marcus, *Spectroscopy*, **2**, 12 (1987).

8 C. L. Chakrabarti, K. L. Headrick, J. C. Hutton, Z. Bicheng, D. C. Bertels and M. H. Bach, *Anal. Chem.*, **62**, 574 (1990).

9 D. S. Gough, P. Hannaford and R. M. Lowe, *Anal. Chem.*, **61**, 1652 (1989).

10 A. E. Bernhard, *Spectroscopy*, **2**, 24 (1987).

11 B. W. Smith, J. B. Womack, N. Omenetto and J. D. Winefordner, *Appl. Spectrosc.*, **43**, 873 (1989).

12 M. Glick, B. W. Smith and J. D. Winefordner, *Anal. Chem.*, **62**, 157 (1990).

13 S. A. Dashin, Yu. A. Karpov, O. A. Kuslyansky, I. A. Mayorov and M. A. Bolshov, *Spectrochim. Acta*, **46B(4)**, 467 (1991).

14 J. P. Deavor, E. Becerra, B. W. Smith and J. D. Winefordner, *Can. J. Appl. Spectrosc.*, **38(1)**, 7 (1993).

15 F Leis, J A C Broekaert and K Laqua, *Spectrochim Acta*, **42B**, 1169 (1987)

16 K Wagatsuma and K Hirokawa, *Anal Chem*, **61**, 2137 (1989)

17 S Caroli, A Alimonte, P Delle Femmine and S K Shukla, *Anal. Chim Acta*, **136**, 225 (1982)

18 K R Hess and W W Harrison, *Anal Chem*, **58**, 1696 (1986)

19 N E Sanderson, E Hall, I Clark, P Charalambous and D Hall, *Mikrochim. Acta*, **1**, 275 (1987)

20 K R Hess, R K Marcus, F L King and W W Harrison, *Anal Chem*, **58**, 1825 (1986)

21 N Jakubowski, D Steuwer and W Vieth, *Anal Chem*, **59**, 1825 (1987)

22 B L Bentz and W W Harrison, *Prog Anal Spectrosc*, **11**, 53 (1988)

23 L F Vassamillet, *J. Anal At Spectrom*, **4**, 451 (1989)

24 R A Kruger, L R P Butler, C J Liebenberg and R G Bohmer, *Analyst*, **102**, 949 (1977)

25 K Wagasuma and K Hirokawa, *Anal. Chem*, **56**, 908 (1984)

26 M S W Webb and R J Webb, *Anal Chim. Acta*, **33**, 138 (1965)

27 O Senoforte, N Violante, F Petrucci and A Alimonte *Spectrochim Acta*, **39B**, 1425 (1984)

28 B M Patel and I D Winefordner, *Can J Appl. Spectrosc*, **32**, 138 (1987)

29 J B Womack, E M Gessler and J D Winefordner, *Spectrochim Acta* **46B**, 301 (1991)

30 S Grazhnlene V Khvostikov and M Sorokin, *Spectrochim Acta*, **46B**, 459 (1991)

31 "The Glow Discharge," F Llewellyn Jones John Wiley & Sons, Inc , New York 1966

32 Z Szilvassy Vamos, J Lazar, M Horvath and A Ketai-Simon, *J Anal At Spectrom.*, **5**, 705 (1990)

33 F Paschen, *Ann Phys* , **50**, 901 (1916)

34 F Paschen, *Ann Phys* , **71**, 142 (1923)

35 Y Takahashi, *Ann. Phys.*, **3**, 49 (1928)

36 R A Sawyer, *Phys Rev* , **36**, 44 (1930)

37 H Schüler, *Z. Phys* , **59**, 149 (1929)

38 H Schüler and H Gollnow, *Z Phys* , **93**, 611 (1935)

39 J R McNally, Jr G R Harrison and E Rowe, *J Opt Soc Am* , **37**, 93 (1947)

40 A Walsh, *Spectrochim Acta*, **7**, 108 (1955)

41 A N Zaidel N I Kalitcevskii, L I Lipis and M P Chuika, "Emission Spectrum Analysis of Atomic Materials," State Publing House of Physicomathematical Literature, Moscow, 1960 US Atomic Energy Commission, AEC-tr-5745, Washington DC, 1963

42 J D Winefordner and T J Vickers, *Anal Chem* , **36**, 805 (1964)

43 W Grimm, *Spectrochim Acta* **23B** 443 (1968)

44 N P Ferreira, H G C Human and L. R P Butler, *Spectrochim Acta*, **35B**, 287 (1980)

45 "Improved Hollow Cathode Lamps for Atomic Spectroscopy," S Caroli, John Wiley & Sons, Inc , New York 1985

46 S Caroli, A Alimonte and F Petrucci, *Anal Chim. Acta* **136** 269 (1982)

47 R. A. Kruger, R. M. Bombella and K. Lagua, *Spectrochim. Acta*, **35B**, 589 (1980)

48 S. Brewer, T. Holbrook, Z. Shi, K. Trivedi and R. Sacks, *Appl. Spectrosc.*, **45**, 1327 (1991)

49 L. McCraig, N. Sesi and R. Sacks, *Appl. Spectrosc.*, **44**, 1176 (1990)

50 T. Araki, J. P. Walters and S. Minami, *Appl. Spectrosc.*, **34**, 33 (1980)

51 P. B. Farnsworth and J. P. walters, *Spectrochim. Acta*, **37B**, 773 (1982)

52 V. A. Novosielov and V. B. Znamenskii, *Spektroskop., Tr. Sib. Soveshch.*, **4th**, 273 (1965), *Chem. Abstr.*, **74**, 18894q (1971)

53 "Gaseous Conductors," James Dillon Cobine, Dover Publications, New York 1958

54 "Electrical Discharges in Gases," F. M. Penning, Philips Technical Library, Eindhoven 1957

55 "Fundamental Processes of Electrical Discharges in Gases," L. B. Loeb, Wiley, NY 1939

56 "Ionized Gases," A. von Engel, Clarendon Press, Oxford 1955

57 R. J. Carman and A. Maitland, *J. Phys. D: Appl. Phys.*, **22**, 1021 (1987)

58 R. J. Carman, *J. Phys. D: Appl. Phys.*, **22**, 55 (1989)

59 R. J. Carman, *J. Phys. D: Appl. Phys.*, **25**, 25 (1992)

60 M. von Stratten and R. Gybels, *Anal. Chem.*, 64, 1855 (1992)

61 A. J. Palmer and J. Wm. McGowan, *J. Appl. Phys.*, **43(10)**, 4084 (1972)

62 T. J. Moratz, *J. Appl. Phys.*, **63(8)**, 2558 (1988)

63 T. C. Paulick, *J. Appl. Phys.*, **67(6)**, 2774 (1990)

64 P. W. J. M. Boumans, *Anal. Chem.*, **44(7)**, 1219 (1972)

65 S E Coe and G G Lister, *J Appl Phys* , **71**, 4781 (1992)

66 M Yu, *J Appl Phys* , **63**, 60 (1988)

67 S Caroli, *J Anal At Spectrom* , **2**, 661 (1987)

68 "The Physics of Fully Ionized Gases," L Spitzer, Wiley, New York 1956

69 J H Ingold, *Phys Rev A*, **43(6)**, 3093 (1991)

70 J H Ingold, *Phys Fluids* **15**, 75 (1972)

71 M Yu, C Kagan, C Cohen and P Avivi, *J Appl Phys* **63(1)**, 60 (1988)

72 "Glow Discharge Processes," B Chapman, John Wiley & Sons, Inc , New York 1980

73 J Vlcek and V Pelikan, *J Phys D Appl Phys* , **22**, 632 (1989)

74 R K Marcus and W W Harrison, *Anal Chem* , **54**, 797 (1986)

75 P Sigmund, *Phys Rev* , **184**, 383 (1969)

76 P Sigmund, *Phys Rev* , **187**, 768 (1969)

77 R V Stuart and G K Wehner, *J Appl Phys* , **33**, 2345 (1962)

78 N Laegrid and G K Wehner, *J Appl Phys* , **32**, 365 (1961)

79 R V Stuart, G K Wehner and G S Anderson, *J Appl Phys* , **40**, 803 (1969)

80 D Ciobotaru, *J Electron. Control* , **17**, 529 (1964)

81 P F Little and A von Engel, *Proc Roy Soc London*, **224A**, 209 (1954)

82 A Guntherschulze, *Z Techn Phys* , **11**, 49 (1930)

83 H Kack and H J Eichler, *J Appl Phys* , **54(9)**, 4939 (1983)

84 C Hirose, Y Adachi and T Makasi, *Appl Spectrosc* , **42(5)**, 815 (1988)

85 F. Howarka and M. Fahl, *Z. Naturforsch*, 27A, 1425 (1972).

86 L. Tonks and I. Langmuir, *Phys. Rev.*, 33, 195 (1929).

87 W. W. Harrison and B. L. Bentz, *Prog. Analyt. Spectrosc.*, **11**, 53 (1988).

88 J. Fletcher and J. R. Cowling, *J. Phys. B*, 6, L258 (1973).

89 A. Lompe, R. Seeliger and E. Wolter, *Ann. Phys.*, **36**, 9 (1939).

90 H. Falk, *Ann. Phys.*, **16**, 160 (1965).

91 E. Badareau, I. Popescu and I. Iova, *Ann. Phys.*, **5**,308 (1960).

92 A. Güntherschultze, *Z. Phys.*, **19**, 313 (1923).

93 A. D. White, *J. Appl. Phys.*, **30**, 711 (1959).

94 T. Kirichenko, V. M. Trachenko and V. B. Tyutyunnik, *Sov. Phys. Tech. Phys.*, **21**, 1080 (1976).

95 C. Hirose, T. Masaki, A. Wada and Y. Adachi, *Appl. Spectrosc.*, **43**, 87 (1989).

96 D. J. Sturges and H. J. Oskam, *J. Appl. Phys.*, **35**, 2887 (1964).

97 "New Trends in Atomic Spectrometric Analysis," J. Czakow, Ossolineum, Wroclaw 1979.

98 R. B. Djulgerova and D. Z. Zhechev, *Spectrosc. Lett.*, **12**, 615 (1979).

99 G. Tolg, *Z. Anal. Chem.*, **294**, 1 (1979).

100 "High Resolution Spectroscopy," S. Tolansky, Methuen, London 1947.

101 K. B. Mitchell, *J. Opt. Soc. Am.*, **51**, 846 (1961).

102 W. G. Schrenk and C. E. Meloan, *Spectrosc. Lett.*, **1**, 237 (1968).

103 K. R. Hess and W. W. Harrison, *Anal. Chem.*, **60**, 691 (1988).

104 B E. Warner, K B Persson and G J Collins, *J. Appl Phys.*, **50**, 5694 (1979)

105 E W. Eckstein, J W Coburn and E Kay, *Int J. Mass Spectrom. Ion Phys.*, **17**, 129 (1975)

106 E Becerra, Ph D Thesis, University of Florida 1992.

107 S Caroli and P Delle Femmine, *Spectrosc Lett.*, **11**, 299 (1978)

108 K Wagatsuma and K Hirokawa, *Spectrochim Acta*, **43B**, 831 (1988)

109 F Chen and J C Williams, *Anal Chem.*, **62**, 489 (1990)

110 J B Ko, *Spectrochim. Acta*, **39B**, 1405 (1984)

111 D S Gough, *Anal Chem.*, **48** 1926 (1976)

112 S Grazhulene, V. Khvostikov and M Sorokin, *Spectrochim Acta* **46B**, 459 (1991)

113 H J Kim and E. H Piepmeier, *Anal. Chem* **60** 2040 (1988).

114 J. C Travis, G C Tuck, R L Watters, Jr , L J Yu and J L Blue, *J Anal. At Spectrom* **6**, 261 (1991)

115 P R Banks and M W Blades *Spectrochim Acta* **44B**, 1117 (1989)

116 J L Tseng, J Y Kung, J. C Williams and S. T Griffin, *Anal Chem*, **64**, 1831 (1992)

117 K Katagowa, T. Uchida and S Minami, *Spectroschim Acta* **36B**, 21 (1981)

118 V Korovin, *Zhur Anal Khim*, **16**, 494 (1961)

119 N Omenetto, *Spectrochim Acta* **44B**, 131 (1989)

120 T Ageki and H Haraguchi, *Anal. Chem*, **62** 81 (1990)

BIOGRAPHICAL SKETCH

Cheryl Morgan was born in Massachusetts and raised and educated in New Hampshire. Prior to her chemistry education, she was a public accountant, a business manager and a professional fundraiser. She received her accounting certificate from the New Hampshire Technical College in 1981. In September of 1986 she went back to college to pursue a degree in chemistry. She received her Bachelor of Science degree from Rivier College in Nashua, N.H., in May of 1989. She entered the University of Florida's graduate school in the fall of 1989. In 1992, she received her M.S. degree from the University of Florida.

I certify that I have read this study and that in my opinion it conforms to acceptable standards of scholarly presentation and is fully adequate, in scope and quality, as a dissertation for the degree of Doctor of Philosophy

James D. Winefordner, Chair
Graduate Research Professor of Chemistry

I certify that I have read this study and that in my opinion it conforms to acceptable standards of scholarly presentation and is fully adequate, in scope and quality, as a dissertation for the degree of Doctor of Philosophy

David H. Powell
Assistant Research Scientist of Chemistry

I certify that I have read this study and that in my opinion it conforms to acceptable standards of scholarly presentation and is fully adequate, in scope and quality, as a dissertation for the degree of Doctor of Philosophy

Robert Kennedy
Assistant Professor of Chemistry

I certify that I have read this study and that in my opinion it conforms to acceptable standards of scholarly presentation and is fully adequate, in scope and quality, as a dissertation for the degree of Doctor of Philosophy

John P. Eyler
Professor of Chemistry

I certify that I have read this study and that in my opinion it conforms to acceptable standards of scholarly presentation and is fully adequate in scope and quality, as a dissertation for the degree of Doctor of Philosophy

Eric R Allen
Professor of Environmental Engineering Sciences

This dissertation was submitted to the Graduate Faculty of the Department of Chemistry in the College of Liberal Arts and Sciences and to the Graduate School and was accepted as partial fulfillment of the requirements for the degree of Doctor of Philosophy.

August, 1993

Dean, Graduate School